Article

Cell Host & Microbe

Dengue Virus Perturbs Mitochondrial Morphodynamics to Dampen Innate Immune Responses

Graphical Abstract

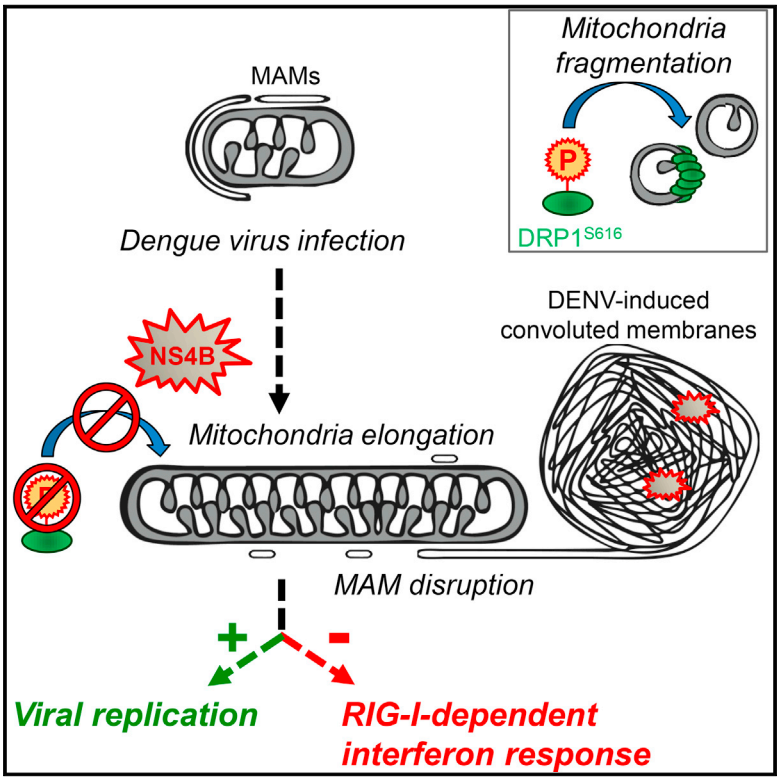

Authors

Laurent Chatel-Chaix, Mirko Cortese, Inés Romero-Brey, ..., Bernd Fischer, Alessia Ruggieri, Ralf Bartenschlager

Correspondence

laurent.chatel-chaix@iaf.inrs.ca (L.C.-C.), ralf.bartenschlager@med.uni-heidelberg.de (R.B.)

In Brief

Chatel-Chaix et al. show that during Dengue virus infection, the viral protein NS4B induces mitochondrial elongation by inactivating the fission factor DRP1. Elongated mitochondria make physical contacts with virus-induced replication factories while mitochondria-associated membranes are altered. Importantly, mitochondria elongation dampens the early interferon response in favor of virus replication.

Highlights

- DENV NS4B induces mitochondria elongation during viral infection
- Elongated mitochondria and virus-induced convoluted membranes are physically linked
- NS4B inhibits activation of the mitochondrial fission factor DRP1
- Mitochondria elongation alleviates DENV-induced RIG-I-dependent innate immunity

Chatel-Chaix et al., 2016, Cell Host & Microbe *20*, 342–356
September 14, 2016
http://dx.doi.org/10.1016/j.chom.2016.07.008

CellPress

Cell Host & Microbe
Article

Dengue Virus Perturbs Mitochondrial Morphodynamics to Dampen Innate Immune Responses

Laurent Chatel-Chaix,[1,*] Mirko Cortese,[1] Inés Romero-Brey,[1,2] Silke Bender,[1] Christopher John Neufeldt,[1] Wolfgang Fischl,[1] Pietro Scaturro,[1] Nicole Schieber,[3] Yannick Schwab,[3] Bernd Fischer,[4] Alessia Ruggieri,[1] and Ralf Bartenschlager[1,2,5,*]

[1]Department of Infectious Diseases, Molecular Virology, Heidelberg University, Im Neuenheimer Feld 345, 69120 Heidelberg, Germany
[2]German Centre for Infection Research, Heidelberg University, 69120 Heidelberg, Germany
[3]European Molecular Biology Laboratory, 69117 Heidelberg, Germany
[4]Computational Genome Biology, German Cancer Research Center (DKFZ), Im Neuenheimer Feld 580, 69120 Heidelberg, Germany
[5]Lead Contact
*Correspondence: laurent.chatel-chaix@iaf.inrs.ca (L.C.-C.), ralf.bartenschlager@med.uni-heidelberg.de (R.B.)
http://dx.doi.org/10.1016/j.chom.2016.07.008

SUMMARY

With no antiviral drugs or widely available vaccines, Dengue virus (DENV) constitutes a public health concern. DENV replicates at ER-derived cytoplasmic structures that include substructures called convoluted membranes (CMs); however, the purpose of these membrane alterations remains unclear. We determine that DENV nonstructural protein (NS)4B, a promising drug target with unknown function, associates with mitochondrial proteins and alters mitochondria morphology to promote infection. During infection, NS4B induces elongation of mitochondria, which physically contact CMs. This restructuring compromises the integrity of mitochondria-associated membranes, sites of ER-mitochondria interface critical for innate immune signaling. The spatio-temporal parameters of CM biogenesis and mitochondria elongation are linked to loss of activation of the fission factor Dynamin-Related Protein-1. Mitochondria elongation promotes DENV replication and alleviates RIG-I-dependent activation of interferon responses. As Zika virus infection induces similar mitochondria elongation, this perturbation may protect DENV and related viruses from innate immunity and create a favorable replicative environment.

INTRODUCTION

Dengue virus (DENV) infection causes the most prevalent arthropod-born viral disease, with an estimated 100 million symptomatic cases per year worldwide, constituting a major unmet medical need. Antiviral drugs are not available, and a vaccine is approved only in a limited number of countries and is not applicable for people at highest risk (namely, young children and the elderly). Around one million DENV-infected individuals develop severe symptoms leading to hemorrhagic fever, shock syndrome and eventually death (Bhatt et al., 2013; World Health Organization, 2009).

DENV is a plus-strand RNA virus belonging to the *Flavivirus* genus of the *Flaviviridae* family. Upon entry into the host cell, the released viral genome is translated at the rough ER, generating a single polyprotein that is processed by host and viral proteases into ten proteins. While the structural proteins Capsid, prM, and Envelope assemble together with the RNA genome into new virus particles, the nonstructural proteins NS1, NS2A, NS2B, NS3, NS4A, NS4B, and NS5 are responsible for the replication of the viral genome. This replication takes place within virus-induced organelle-like cytoplasmic structures called replication factories (Acosta et al., 2014; Chatel-Chaix and Bartenschlager, 2014). These ER-derived membranous compartments consist of three substructures: (1) vesicle packets (VPs), formed by invagination of the ER membrane and believed to be the site of RNA replication; (2) virus "bags" in which virions accumulate most often in regular arrays; (3) convoluted membranes (CMs) that form by an unknown process (Welsch et al., 2009). Owing to the enrichment of NS3 in CMs, they are considered to play a role in polyprotein maturation (Welsch et al., 2009; Westaway et al., 1997). However, DENV RNA translation occurs at the rough ER where (co-translational) polyprotein cleavage occurs, arguing that CMs most likely play additional role(s). While there is evidence that NS4A is able to induce CMs to some extent (Miller et al., 2007), other DENV proteins, such as NS3 or NS4B, might contribute to this process. In addition to this ER remodeling activity, DENV proteins were also shown to interfere with specialized cellular processes in order to create an environment favorable to viral RNA replication. This includes a role of NS4A in autophagy (McLean et al., 2011) and modulation of RNAi, as well as innate immunity signaling by NS4B (Dalrymple et al., 2015; Kakumani et al., 2013; Muñoz-Jordan et al., 2003, 2005). However, no functional link between these co-opting activities and the viral replication factories has been established so far.

The functions of NS4B might be of particular clinical relevance since this DENV protein has been identified as target of several antiviral compounds, some of which are currently in preclinical development (reviewed in Xie et al., 2015). To gain more insight into NS4B function(s) during DENV infection, we determined the

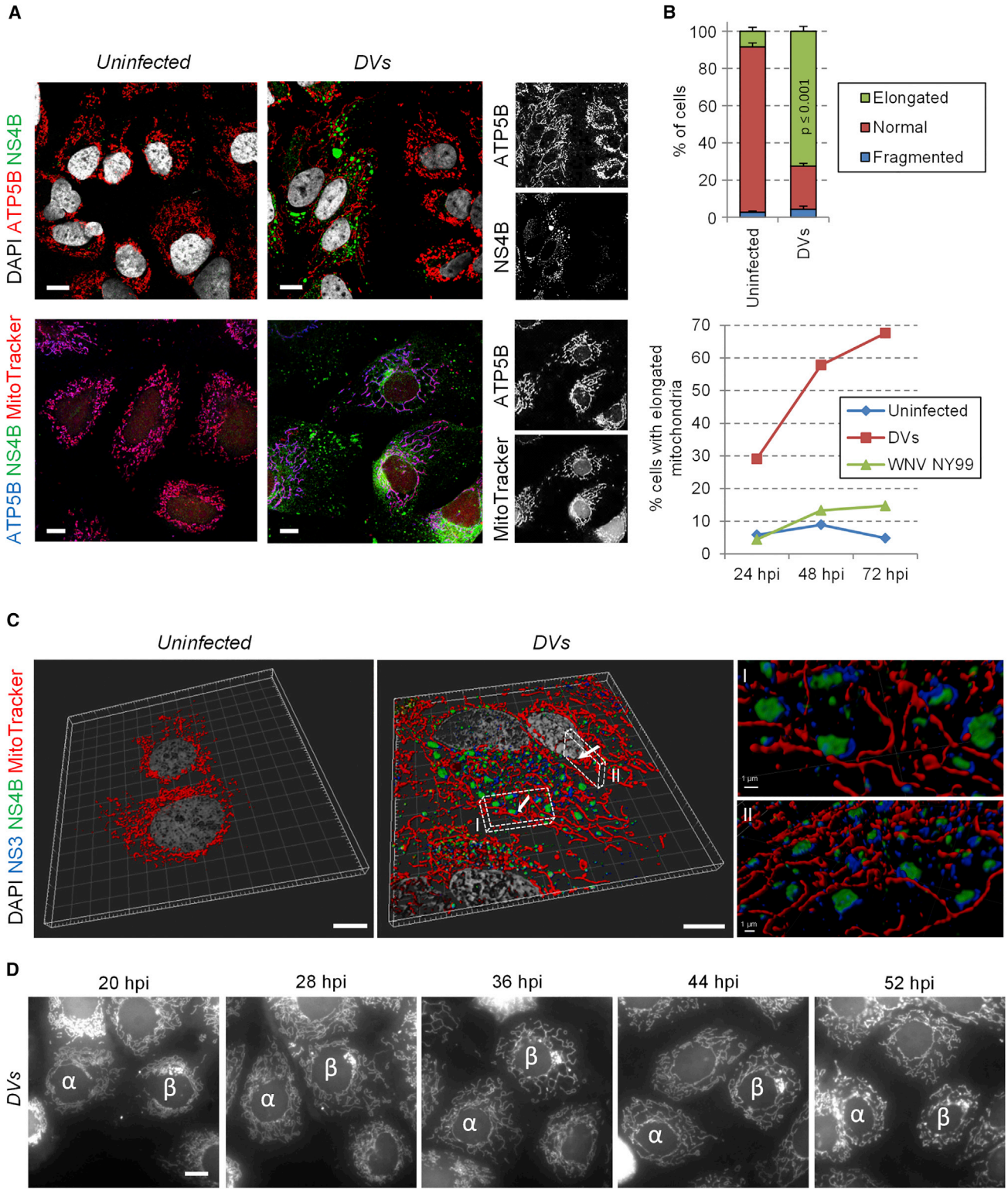

Figure 1. DENV Infection Induces Mitochondria Elongation

(A) Huh7 cells were infected with the DENV2 strain 16681 (DVs) at MOI = 1 or left uninfected. Three days later, cells were fixed, permeabilized, and indicated proteins were visualized by immunofluorescence using confocal microscopy. Incubation with MitoTracker was performed right before fixation.

(B) Quantification of immunofluorescence shown in (A). Upper panel: the mitochondrial network of ~100 cells per condition and experiment (n = 4) was examined and classified into three morphological categories (normal, fragmented, elongated). Lower panel: the morphology of the mitochondrial network was analyzed in uninfected, DVs- or WNV-infected cells at 1, 2, and 3 days post infection. Error bars indicate SEM calculated using four independent experiments.

(legend continued on next page)

NS4B-specific host interactome in infected cells and identified several mitochondrial components. We show that DENV infection perturbs mitochondrial morphodynamics by inducing mitochondria elongation at the vicinity of NS3- and NS4B-containing CMs. Elongation is induced by NS4B and mediated by inactivation of the mitochondrial fission factor Dynamin-Related Protein-1 (DRP1). Importantly, mitochondria elongation favors DENV replication and dampens activation of the interferon response.

RESULTS

DENV Infection Induces Mitochondrial Elongation

With the aim to discover functions of NS4B, we elucidated the host interactome of NS4B in DENV-infected cells by taking advantage of a previously reported DENV2 16681 (DVs) strain that expresses a fully functional HA-tagged NS4B (Figure S1A) (Chatel-Chaix et al., 2015). NS4B-HA*-associated proteins were efficiently co-purified from infected Huh7 hepatoma cells (Figures S1B and S1C) and identified using mass spectrometry (Figure S1D; Table S1). Based on three independent preparations, 19 host proteins were significantly enriched with NS4B-HA* and very strikingly, 12 of these hits were mitochondrial proteins. Among those, ATP synthase β subunit (ATP5B), monoamine oxidase B (MAOB), and voltage-dependent anion channel 2 (VDAC2) were validated as NS4B interaction partners (Figure S1E), arguing for an association between NS4B and mitochondria.

Immunofluorescence-based labeling of these host cell proteins combined with whole mitochondria staining using MitoTracker revealed that the morphology of mitochondria drastically changed in DVs-infected cells (Figures 1A and 1B; Figure S1F). Indeed, as confirmed by confocal microscopy-based 3D reconstruction of DENV-infected cells (Figure 1C; Movie S1), mitochondria were elongated and frequently in physical contacts with punctate structures that contained both NS3 and NS4B but not the replication intermediate double strand (ds)RNA (Figure S2A), suggesting that these structures are not vesicle packets, the presumed site of viral RNA replication. The same elongation phenotype was observed with another DENV2 strain, New Guinea C (NGC), with DENV of other serotypes (1, 3, and 4) and with two strains of the closely related Zika virus (ZIKV; H/PF/2013 and MR766, belonging to the Asian and the African lineage, respectively) (Figures S2B–S2G and S2J). In contrast, no such alteration was observed in cells infected with other *Flaviviridae* members, namely the flavivirus West Nile virus (WNV) and the hepacivirus hepatitis C virus (HCV) (Figure 1B; Figures S2H–S2J), arguing that this phenotype is specific to DENV and ZIKV.

Next, we generated a Huh7 cell line expressing a mitochondria-targeted fluorophore (mito-mTurquoise2), allowing live cell imaging of mitochondrial morphodynamics. This cell line supported DENV replication comparably to the parental Huh7 cell line and recapitulated mitochondria morphology changes when analyzing fixed cells (Figures S3A and S3B). In living uninfected cells, the mitochondrial network was highly dynamic, and mitochondrial morphology alternated between moderate elongation and fragmentation (Figure S3C; Movie S2). In stark contrast, in DVs-infected cells, mitochondria elongation became first visible 23 hr after infection and was most pronounced between 35 and 50 hr post infection (Figure 1D; Movie S2). At very late time points after infection, the mitochondrial network collapsed concomitantly with cell death due to DENV-induced-cytopathic effects. Mitochondria elongation was also observed in DENV2 NGC-infected cells (Movie S3), but with a faster kinetic correlating with a higher replication capacity of this strain. These observations clearly demonstrate that DENV infection modulates mitochondrial morphodynamics.

Elongated Mitochondria and NS3/NS4B-Containing CMs Are Physically Linked

To characterize the ultrastructural details of elongated mitochondria in DENV-infected cells, we utilized automated serial imaging by focused ion beam–scanning electron microscopy (FIB-SEM). Three-dimensional reconstruction of most of the cell volume revealed a network of elongated mitochondria in both NGC- and DVs-infected cells, which was not found in uninfected cells (Figure 2A; Figure S4A; Movie S4). Elongated mitochondria often localized in the vicinity of electron dense structures resembling convoluted membranes. Indeed, examination of ultrathin sections of infected cells at a higher resolution by transmission electron microscopy (TEM) confirmed that CM-proximal mitochondria were more elongated than CM-distal ones (Figure 2B–E). In contrast to uninfected cells in which mitochondria were found in contact with ER tubules called mitochondria-associated membranes (MAMs) (Vance, 2014), this interface was mostly disrupted in DENV-infected cells. Very strikingly, CMs appeared to be physically connected to mitochondria only at single sites arguing for a profound loss of the mitochondria–ER interface (Figure 2B; Figure S4B, red arrows).

To further confirm this DENV-mediated alteration of the ER–mitochondria interface at the whole cell level, we generated a Huh7 cell line stably expressing mito-mTurquoise2 and a fluorescent ER marker (YFP-Sec61β). This allowed us to identify ER-mitochondria contact sites using confocal microscopy as previously described (Friedman et al., 2011). DENV replicated efficiently in this cell line and induced mitochondria elongation (Figures S3D and S3E). Use of 3D co-localization analysis following reconstruction of mitochondria and Sec61β-positive ER networks showed that the extent of contacts between these two compartments was significantly altered in DENV-infected cells (Figures 2F and 2G; Figures S5A and S5B), arguing that DENV profoundly altered the MAMs.

Interestingly, Sec61β accumulated in infected cells in NS3-positive large structures (Figure S3E, right panel) corresponding to the dsRNA-free NS3/NS4B-containing punctae described in

(C) Upon optical sectioning and deconvolution, Z-stacks were used for 3D reconstruction of control and DVs-infected cells stained for NS3, NS4B, and mitochondria. (I and II) Magnifications of regions of interest (indicated with white cuboids) show the proximity between NS3/NS4B-containing punctae and elongated mitochondria. The viewing angles are indicated with the white arrows in the cuboids.

(D) Live cell imaging frame captures of DVs-infected Huh7 cells (MOI = 10) expressing a mitochondria-targeted mTurquoise2 fluorophore. Captures were made 20, 28, 36, 44, and 52 hr post infection and show progressive elongation of mitochondria over time. To facilitate tracking, two cells of interest are labeled with α and β. Scale bar, 10 μm, except (CI) and (CII).

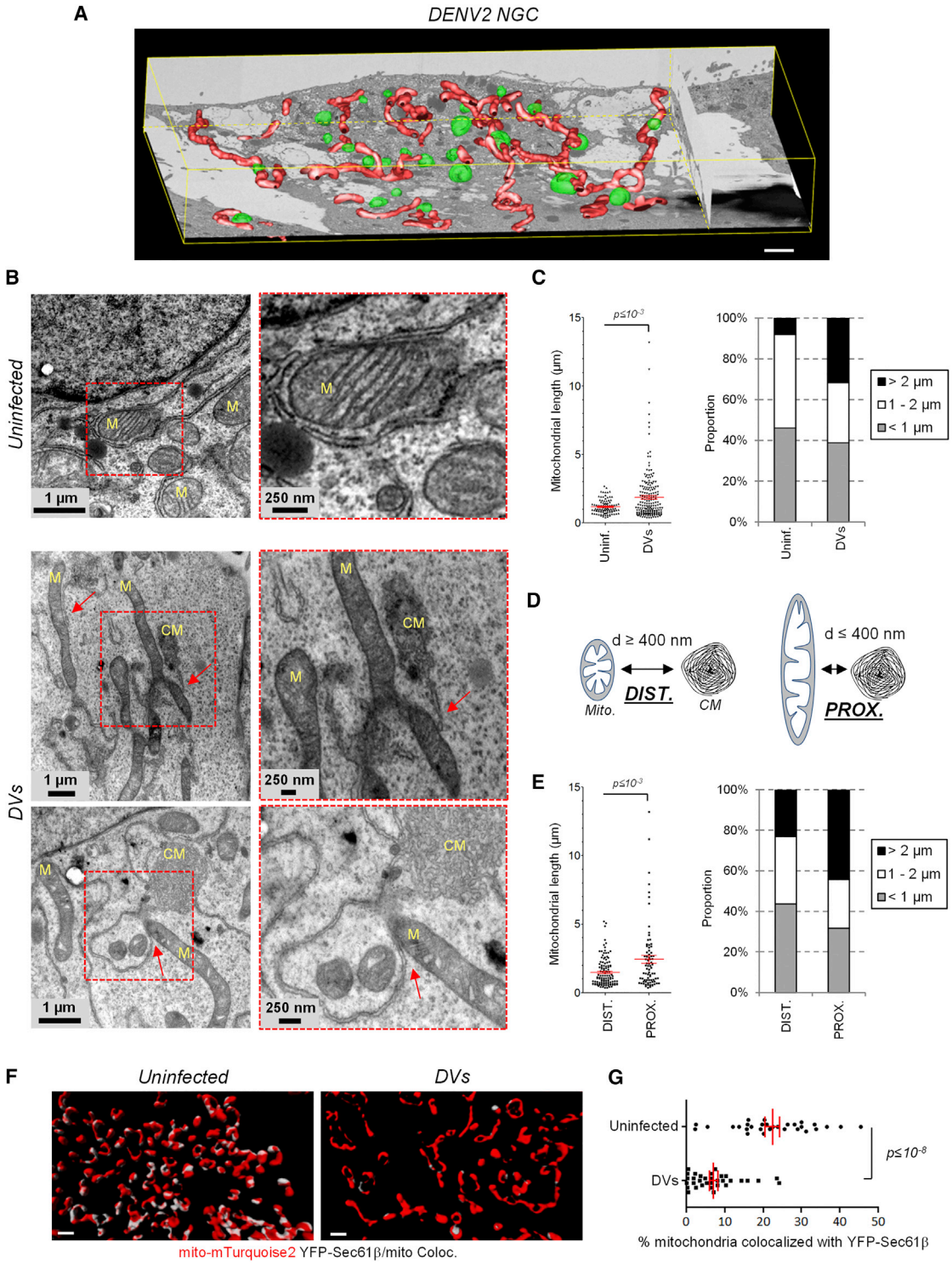

Figure 2. DENV2 Induces Mitochondria Elongation in the Vicinity of Viral Convoluted Membranes and Alters Mitochondria-ER Contacts

(A) Huh7 cells were infected with DENV2 NGC (MOI = 5). 24 hr later, cells were processed for FIB/SEM. Tridimensional reconstruction for mitochondria (red) and CM (green) was performed. Scale bar, 2 µm.

(B) Sections of control and DVs-infected cells were analyzed by TEM. Magnification of regions of interest, red squares) are given below each top panel to highlight that ER-mitochondria contacts sites are mostly disrupted. In addition, CMs are connected to mitochondria (M) at distinct sites via ER membranes (red arrows).

(C) The length of mitochondria was measured with the ImageJ software package using multiple images acquired by TEM; lengths were classified into three categories.

(legend continued on next page)

Figures 1C and S2A. Therefore, we hypothesized that these mitochondria-connected puncta might be CMs. We evaluated this assumption in several ways. First, we used TEM of immunolabeled thawed cryosections of DVs-infected cells and confirmed that CMs contained both NS3 (as previously reported by Welsch et al., 2009) and a fraction of NS4B (Figures 3A–3C). Second, we applied correlative light-electron microscopy (CLEM) of DENV-infected cells using the Huh7/mito-mTurquoise2/YFP-Sec61β cell line previously described. Importantly, by using YFP-Sec61β as an indirect marker of NS3/NS4B-containing puncta to perform CLEM with nonpermeabilized cells, the YFP-Sec61β fluorescent signal perfectly correlated with CMs detected by TEM, but not with VPs (Figures 3D–3F; Figures S5C–S5E). This result unambiguously identified the puncta containing both NS3 and NS4B, but devoid of dsRNA as DENV-induced CMs.

Taking advantage of this Huh7/mito-mTurquoise2/YFP-Sec61β cell line, we characterized the spatiotemporal relationship between mitochondria elongation and CM biogenesis by live-cell imaging of infected cells (Movies S5 and S6). Cells with CMs were detectable as early as 21 hr post infection and accumulated over time (Figure 3G). 86% of the cells with CMs also showed a network of elongated mitochondria (Figure 3H). Morphology of CMs was highly dynamic and merging as well as division of CMs was observed (Figure S6A; Movie S6). Notably, in 36% of infected cells (i.e., 42% of those also displaying elongated mitochondria) formation of CMs and mitochondria elongation occurred simultaneously. Moreover, contacts between these two compartments were readily detectable throughout the infection (Figure S6B). Taken together, these results suggest a spatio-temporal relationship between CM biogenesis and mitochondrial morphodynamics.

Expression of DENV NS4B Is Sufficient for Mitochondria Elongation

Next, we aimed at determining the DENV protein responsible for altering mitochondria morphodynamics. We used an expression-based approach (Figure 4A) and took into account that DENV nonstructural proteins are sufficient for mitochondrial elongation, because we observed this phenotype in cells containing a DENV2 subgenomic replicon or expressing the NS1-5 polyprotein from a transfected plasmid (Figures 4B and 4C). Because several mitochondrial proteins were identified in the NS4B interactome, we hypothesized that NS4B was responsible for mitochondria elongation. Indeed, this phenotype was recapitulated when NS4B was expressed either as a NS4A-2K-NS4B precursor or as 2K-NS4B protein, with 2K serving as signal sequence for proper membrane insertion of NS4B (Figures 4D and 4E) (Chatel-Chaix et al., 2015). In contrast, individual expression of NS4A, NS2B-3, or the HCV NS3-5B polyprotein did not induce mitochondria elongation, demonstrating that this phenotype is specific to DENV NS4B (Figures 4C–4E).

Mitochondria Elongation Favors DENV Replication

Mitochondria morphology is highly dynamic and relies on a fine-tuned equilibrium between fusion and fission leading to elongation and fragmentation, respectively. These processes are controlled by fusion factors (e.g., optic atrophy 1 [OPA1] and the mitofusins MFN2 and MFN1), as well as by fission factors (e.g., DRP1 and mitochondrial fission factor [MFF]) (Smirnova et al., 2001; Smirnova et al., 1998; Otera et al., 2010; Chen et al., 2003; Olichon et al., 2003). While mitochondria-resident proteins MFN and OPA1 localize on the outer and inner mitochondrial membranes, respectively, and promote interorganelle membrane fusion, DRP1 is primarily cytosolic and translocated to mitochondria to mediate fragmentation via its dynamin-related activity (Chan, 2012). This fusion/fission equilibrium can be influenced by modulating the expression of these factors. Indeed, RNAi-mediated knockdown of DRP1 stimulated mitochondria elongation, whereas decreased MFN2 expression favored their fragmentation (Figures 5A and 5B) without affecting cell viability during a 5-day observation period (Figure 5C). Importantly, DRP1 knockdown-mediated elongation stimulated replication of both DENV strains DVs and NGC (Figures 5D–5F), whereas MFN2 knockdown-enforced mitochondria fragmentation inhibited DENV replication. Interestingly, the replication of ZIKV, which also induced mitochondria elongation, was stimulated by DRP1 knockdown as well (Figures 5G and S6C), whereas replication of WNV and HCV remained unaffected under these conditions (Figures 5H and S6C). These results show that mitochondria elongation favors DENV and ZIKV replication.

To directly address the impact of enforced mitochondrial morphodynamics on CM morphogenesis, we exploited a NS1-5 polyprotein-based expression system to study the impact of DRP1 or MFN2 knockdown on frequency and size of NS4B punctae independent from viral replication (Figures 5I–5K). Enforced mitochondria elongation by silencing DRP1 expression increased the number and volume of NS4B-containing clusters whereas in cells with MFN2 knockdown no NS4B-positive clusters (and hence, CMs) could be detected. Interestingly, rapid induction of mitochondria fragmentation via CCCP-mediated depolarization resulted in a loss of NS4B-containing CMs (Figure S7A). Altogether, these data support the notion that mitochondria morphology directly influences the biogenesis or stability of CMs.

DENV NS4B Inhibits DRP1 Activation

We next sought to determine the molecular mechanism underlying DENV-induced mitochondria elongation. In the first set of experiments, we determined the stoichiometries between DRP1

(D and E) Elongation of CM-proximal mitochondria. The distance between mitochondria and CMs (d) was measured. When this distance was below or above 400 nm, a given mitochondria was considered proximal (PROX.) or distal (DIST.), respectively. Mitochondria lengths (y axis) of these two groups are shown and were classified as in (C). Further examples of EM images are given in Figure S4B.

(F) Huh7/mito-mTurquoise2/YFP-Sec61β cells were left uninfected or infected with DVs. Three days later, cells were fixed and stained for NS3 (not shown). Optical sections were acquired with a spinning disc confocal microscope and after deconvolution, Z-stacks were used for 3D reconstruction and 3D colocalization analysis between mitochondria and YFP-Sec61β-containing ER networks. Note that NS3-positive cells were considered infected. White areas on reconstructed mitochondria indicate sites of colocalization with YFP-Sec61β (Coloc.). Scale bar, 1 μm.

(G) A 3D colocalization analysis quantifying the extent of mitochondria/Sec61β contacts in uninfected (n = 30) and DVs-infected cells (n = 33).

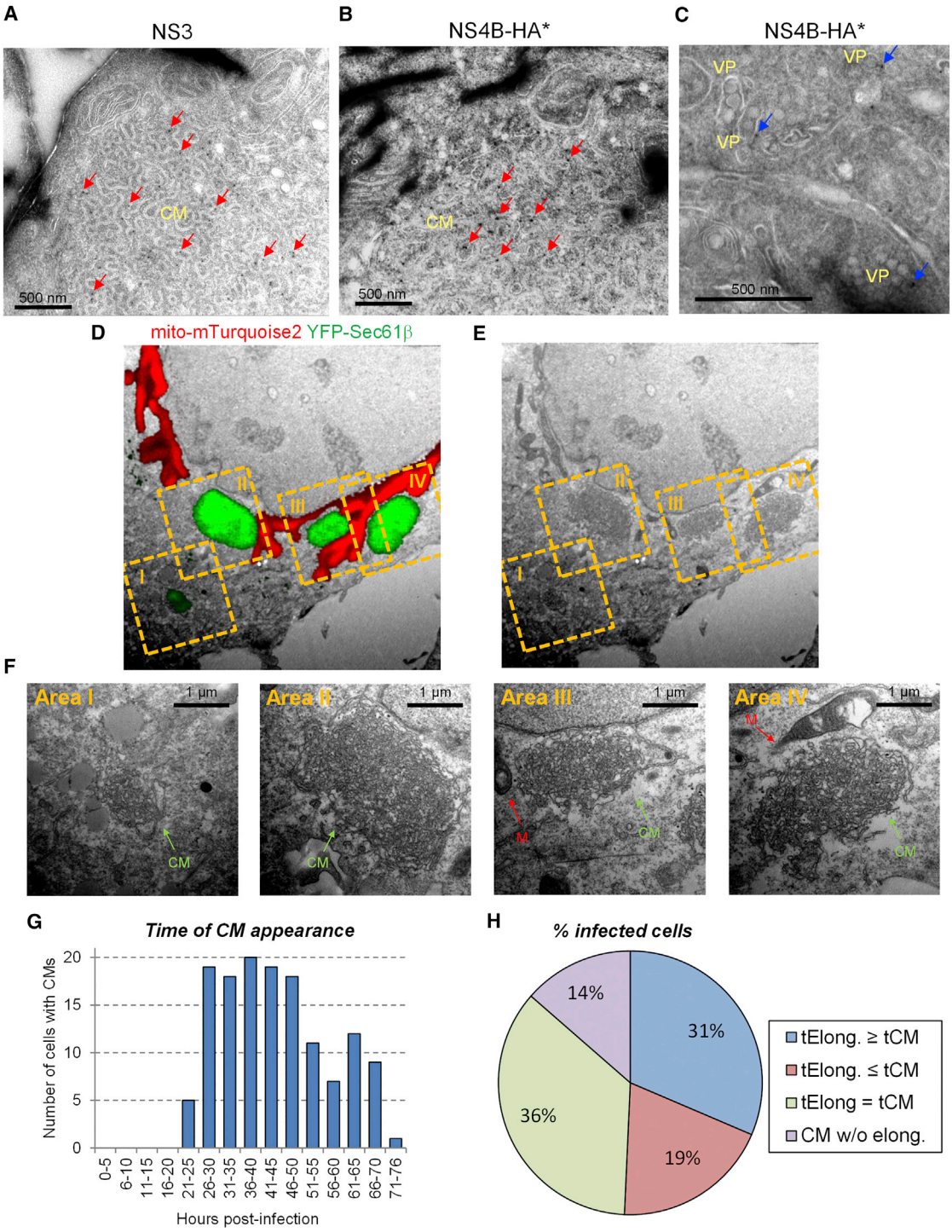

Figure 3. CMs Contain Both NS4B and NS3, and Their Biogenesis Is Linked in Time and Space with Mitochondria Elongation in DENV-Infected Cells

(A–C) Huh7 cells were infected with DVs(NS4B-HA*). Three days post infection, cells were processed for immunolabeling of thawed cryosections using NS3- or HA-specific primary antibodies to detect NS3 (A) or NS4B-HA* (B and C), respectively. Red arrows: immune-gold-labeled NS3 (A) or NS4B-HA* (B) within DENV-induced CMs. Blue arrows: immune-gold-labeled NS4B-HA* (C) associated with VPs.

(D–F) Huh7/mito-mTurquoise2/YFP-Sec61β cells were infected with DVs and processed for CLEM three days post infection. The mitochondria signal and NS3/NS4B-containing YFP-Sec61β puncta are shown in red and green, respectively. Mitochondria morphologies were used to allocate the red fluorescent signal of a Z-stack to the proper ultrastructure of the EM image and hence, for overall correlation. Regions of interest, yellow dashed squares, were selected for higher magnification analyses that are shown in (F).

(legend continued on next page)

and the fusion factors MFN1, MFN2 and OPA1. Their expression levels remained unchanged upon DENV2 infection (Figure S7B) and hence, alterations in their relative abundance could not account for DENV-induced mitochondria elongation. In uninfected cells, DRP1 is detectable only as puncta localizing preferentially at the tip of daughter mitochondria, reflecting DRP1 oligomers mediating or having resolved the fission of a mitochondrion (Figure 6A; Figure S7C) (Strack and Cribbs, 2012). Importantly, in cells infected with DVs or NGC, mitochondria-associated DRP1 levels decreased (Figures 6A and S7D, respectively), suggesting that DRP1 translocation to mitochondria and hence, their fragmentation is altered.

Since serine phosphorylation of DRP1 at residues 616 and 637 can stimulate and repress DRP1 fission activity, respectively (reviewed in Chan, 2012; Lee and Yoon, 2014), we evaluated whether DENV infection influences DRP1 phosphorylation status. While phosphorylation of Ser637 remained unaffected during infection, the level of DRP1 phosphorylated at serine residue 616 decreased in DENV-infected cells for both endogenous and overexpressed DRP1 (Figures 6B–6C and S7E). Ser616 of DRP1 was previously reported to be phosphorylated by several kinases, namely CDK1, CDK5, and ERK1/2 (Lee and Yoon, 2014; Chan, 2012). Strikingly, CDK1 expression decreased in DENV-infected cells (Figure 6D) while the levels of activated ERK1/2 and CDK5 remained unchanged during DENV infection (Figure S7E). Importantly, this phenotype was mediated by properly membrane-associated NS4B since the expression of either the NS4A-2K-NS4B precursor or 2K-NS4B alone was sufficient to decrease both P-Ser616-DRP1 and CDK1 levels, which was not the case with NS4B lacking the 2K signal sequence (Figure 6E). These results demonstrate that DENV inhibits phospho-S616-dependent activation of DRP1 and its subsequent translocation to mitochondria, thus perturbing the fusion/fission equilibrium. This result provides an explanation for mitochondria elongation in virus-infected cells.

Mitochondria Elongation Alleviates DENV-Induced Innate Immunity

The ER–mitochondria interface serves as platform for MAVS-dependent innate signaling through the recruitment of activated cytosolic RNA sensors RIG-I and MDA5 (Horner et al., 2011). In the light of the altered ER-mitochondria contact sites, indicative of MAMs, we reasoned that the virus might induce mitochondrial changes in DENV-infected cells to suppress the activation of the innate antiviral response. Hence, we evaluated the impact of mitochondria morphology on DENV-induced interferon (IFN) induction. When elongation was favored by knockdown of DRP1 expression in Huh7 cells, the induction of endogenous IFN-λ1 expression markedly decreased, best visible with the DENV2 NGC strain (Figure 7A), consistent with the increase of virus titer (Figures 5E and 5F). In contrast, knockdown of MFN2 expression induced mitochondria fragmentation and enhanced the expression of IFN-λ1 (Figure 7A), which correlated with the impaired DENV replication (Figures 5E and 5F). The analogous result was obtained when monitoring IFN-λ1, IFN-β and ISG56 expression in A549 cells (Figure 7B), which are more competent especially with respect to IFN-β production. Interestingly, knockout of RIG-I in Huh7 cells by CRISPR/Cas9 technology suppressed DENV-induced IFN-λ1 production ~100-fold (Figures 7D and 7E), showing that RIG-I-dependent signaling is responsible for most of DENV-induced innate immune response.

Considering the links among MAMs, CMs, and elongated mitochondria, we hypothesized that mitochondria elongation might impair DENV-induced RIG-I translocation to MAMs, thus dampening innate immunity. We altered mitochondria morphology by knockdown of DRP1 and MFN2 and isolated MAMs by subcellular fractionation. Upon knockdown of DRP1 expression, the abundance of RIG-1 in the MAM fraction was drastically decreased, concomitant with an accumulation in the cytosolic fraction (Figure 7F) and consistent with a reduced innate immune signaling (Figure 7A). Consistently, the opposite phenotype was observed upon silencing of MFN2 expression. Overall, these data demonstrate that mitochondria elongation alleviates DENV-induced RIG-I-dependent innate immunity and further suggest that DENV-induced mitochondria elongation confers a protective effect against these antiviral responses.

DISCUSSION

It is well established that all plus-strand RNA viruses induce membranous replication factories (Paul and Bartenschlager, 2013), but the impact of these factories on morphology and function of cellular organelles remains largely unknown. Here, we show that DENV—via NS4B—induces mitochondria elongation as a result of fragmentation inhibition. This was due to suppressed phosphorylation-dependent activation of DRP1 and impaired translocation to mitochondria, which, however, is required to trigger fission via the dynamin-related activity residing in DRP1. The sole expression of 2K-NS4B is sufficient to downregulate CDK1, a kinase contributing to DRP1 phosphorylation at Ser616; this is consistent with the observed induction of mitochondria elongation by this viral protein. Since CDK1 (in complex with cyclin B) is primarily active during mitosis, NS4B might inhibit DRP1 phosphorylation predominantly during this phase of the cell cycle. In this case, the alteration of mitochondria morphology during interphase as observed here would be triggered during mitosis and last for extended periods thereafter.

By using a replication-independent DENV NS1-5 polyprotein expression system, we provide evidence that mitochondria morphology directly influences NS4B large puncta, reminiscent of CMs (Figures 5J and 5K). Consistently, rapid induction of mitochondria fragmentation by CCCP treatment led to the disappearance of NS4B-containing CMs (Figure S7A), supporting the notion that mitochondria morphology is important for CM biogenesis and/or maintenance. However, CMs were not detected in cells expressing only 2K-NS4B (M.C., L.C.-C., and

(G and H) Huh7/mito-mTurquoise2/YFP-Sec61β cells were infected with DVs (MOI = 10) and analyzed by live-cell imaging. For 140 cells from 13 movies, the time of first appearance of CMs was determined (G) and correlated with the time when a given mitochondrial network started to elongate. Cells in which YFP-Sec61β accumulated within puncta were considered infected with DENV. (H) Infected cells were classified into four defined categories: tElong. ≥ tCM: Mitochondria elongation occurred after CM appearance; tElong. ≤ tCM: CM appeared after mitochondria elongation; tElong. = tCM. The two processes occurred simultaneously. CM w/o elong.: CM formation without detectable mitochondria elongation.

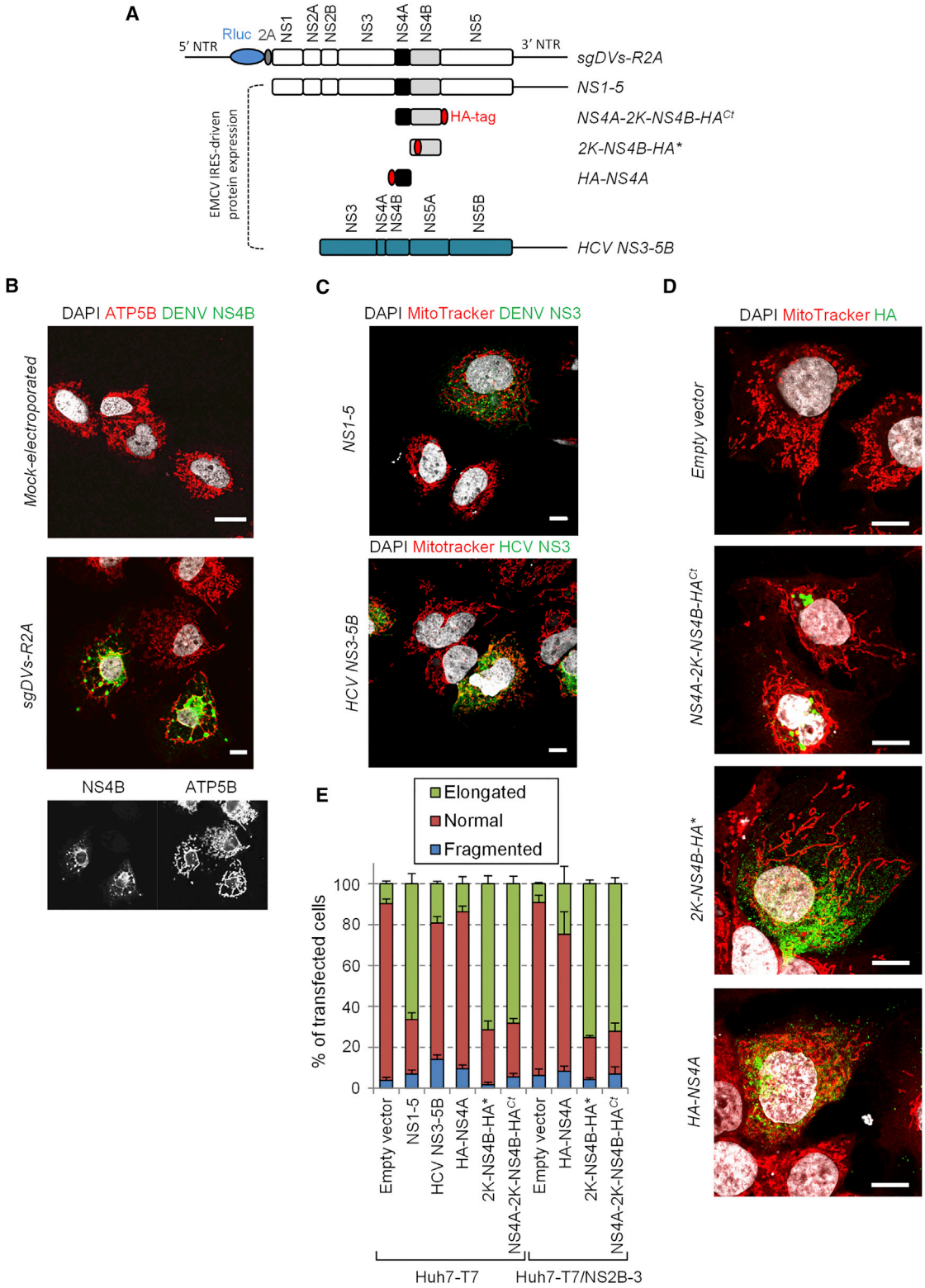

Figure 4. DENV2 NS4B Induces Mitochondria Elongation

(A) Schematic representation of used constructs. The subgenomic replicon is depicted in the top. The constructs used for expression with the T7-based system are indicated below. Black lines represent the DENV and HCV untranslated regions (NTRs). The HA-tag is shown as red oval.

(B) Huh7 cells were electroporated with capped in vitro transcripts of a sub-genomic RNA. Three days later, cells were processed for detection of ATP5B and DENV NS4B by immunofluorescence using confocal microscopy.

(legend continued on next page)

R.B., unpublished data), arguing that CMs are not absolutely required for mitochondria elongation and that CM biogenesis requires additional viral factors, such as NS4A (Miller et al., 2007).

Several reports showed that DRP1 translocation to mitochondria depends on prior actin-dependent constriction of mitochondria by juxtaposed ER tubules or, more precisely, MAMs (Friedman et al., 2011; Korobova et al., 2013; Manor et al., 2015). Considering that ER-mitochondria contacts are partly disrupted in DENV-infected cells, we hypothesize that CMs also contribute to the disappearance of pre-constricting ER and hence, to the loss of DRP1 translocation and mitochondria fission. Hence, the observed mitochondria elongation most probably results from a combination of NS4B-dependent inactivation of DRP1 and MAM disruption that appears to be linked to CM biogenesis. However, we cannot exclude that the fusion machinery might be modulated by DENV as well, e.g., by altering MFN proteins (Pyakurel et al., 2015; Chen and Dorn, 2013; Glauser et al., 2011; Leboucher et al., 2012; Ziviani et al., 2010). Very recently, Yu and colleagues proposed that DENV infection inhibits fusion activity of mitofusin proteins (Yu et al., 2015). Although we never detected MFN1 or MFN2 cleavage in DENV-infected cells, we note that the conclusions of Yu and coworkers were based on rather artificial experimental approaches, including heterokaryon formation and MFN overexpression-based mitochondria hyperfusion assays, and the impact of DENV on mitochondria fusion was evaluated during short timescales and after high virus-dose inoculation. Moreover, these authors used stable knockdown cell lines to silence MFN gene expression, which we avoided to limit the risk of selecting for cells compensating the fragmentation phenotype by alternative mechanisms to maintain the fusion/fission equilibrium. Moreover, Yu and colleagues did not directly address the impact of DENV on DRP1 function and on general mitochondria morphodynamics (e.g., by using mitochondria staining of naive cells infected with DENV). We note that Yu and colleagues did not report mitochondria fragmentation in DENV-infected cells, which would be expected in case of fusion inhibition; this demonstrates that the proposed impairment of fusion makes little, if any, contribution to the overall mitochondria morphology in infected cells. Some of the discrepancies might also be explained by different timing of analyses. While the DENV-induced elongation phenotype reported here is most obvious 48–72 hr post infection when CMs form, Yu and coworkers observed MFN function as early as 24 hr post infection.

The temporal analysis of CM biogenesis revealed that in 36% of infected cells, mitochondria elongation occurs simultaneously to the appearance of CMs. While these two phenomena are most probably not strictly interdependent, our data argue for a spatio-temporal coordination between these processes. Consistently, 86% of cells contained both elongated mitochondria and CMs that remained in close proximity throughout the course of infection.

During the last decade, the ER-mitochondria interface has emerged as a critical signaling platform for MAVS-dependent activation of the innate immune response (Horner et al., 2011; van Vliet et al., 2014). We show that mitochondria elongate during DENV infection, and ER-mitochondria contact sites are disrupted most probably by CM formation. In this way, ER membranes tightly surrounding mitochondria appear to be removed, thus impairing the recruitment of activated RIG-I to MAMs and protecting the virus from an antiviral state. While this is an interesting mechanism by which a virus escapes innate antiviral defense, DENV utilizes additional strategies. For instance, the DENV NS2B-3 protease, is highly enriched in CMs, proteolytically inactivates the MAM-resident signaling adaptor STING (Aguirre et al., 2012; Yu et al., 2012) and prevents RIG-I translocation to mitochondria by targeting the adaptor protein 14-3-3ε (Chan and Gack, 2016). Moreover, NS4B overexpression was found to impair the RIG-I/MDA5-dependent pathway at the level of TBK1/IKKε activation via an unknown process (Dalrymple et al., 2015). Given the central role of NS4B in mitochondria elongation as described here and its interaction with NS3 (Chatel-Chaix et al., 2015), the functional cross-talk between these two proteins for all these phenotypes will be an important task for future studies.

Despite conflicting reports about the role of mitofusins in IFN induction (Castanier et al., 2010; Onoguchi et al., 2010; Yasukawa et al., 2009; Yu et al., 2015), it was shown that mitochondria elongation increases ER-mitochondria contacts (as monitored by STING/MAVS interaction) and would hence, stimulate innate immune signaling (Castanier et al., 2010). Moreover, several studies support the idea that some viruses evade from innate immunity by inducing mitochondria fragmentation to disrupt MAVS-dependent signaling (Kim et al., 2014; Yoshizumi et al., 2014; Xia et al., 2014). In the present study, we rather observe that mitochondria elongation is proviral and alleviates type I and III IFN expression. This discrepancy might be due to the fact that DENV, by inducing CMs, disrupts MAMs and thus, an early IFN response. Reminiscent to DENV, Shi and colleagues reported that severe acute respiratory syndrome-coronavirus (SARS-CoV) ORF-9b protein induces mitochondria elongation through the proteasomal degradation of DRP1, and impairs innate immunity by targeting MAVS-dependent signaling (Shi et al., 2014). Of note, two independent studies by other groups showed that SARS-CoV also induces convoluted membranes (Knoops et al., 2008) and impairs STING-dependent signaling (Sun et al., 2012). In light of our results with DENV, one might speculate that SARS-CoV uses a similar ''mitochondria-elongation'' strategy to disrupt innate immunity. Although some molecular details about the link of mitochondria elongation

(C and D) Huh7 cells stably expressing T7 RNA polymerase only (Huh7-T7) (C and D) or T7 RNA polymerase and DENV NS2B-3 (Huh7-T7/NS2B-3) (not shown) were transfected with the expression constructs specified in the left of each panel. 24 hr later, cells were incubated with MitoTracker, fixed, immunostained for the indicated proteins and analyzed by confocal microscopy. Scale bar, 10 μm.

(E) Based on the analysis of mitochondria morphology of at least 150 cells per condition and at least three independent experiments, cells were classified into three groups as follows: elongated, normal and fragmented mitochondrial network. Error bars indicate SEM calculated using three or four independent experiments.

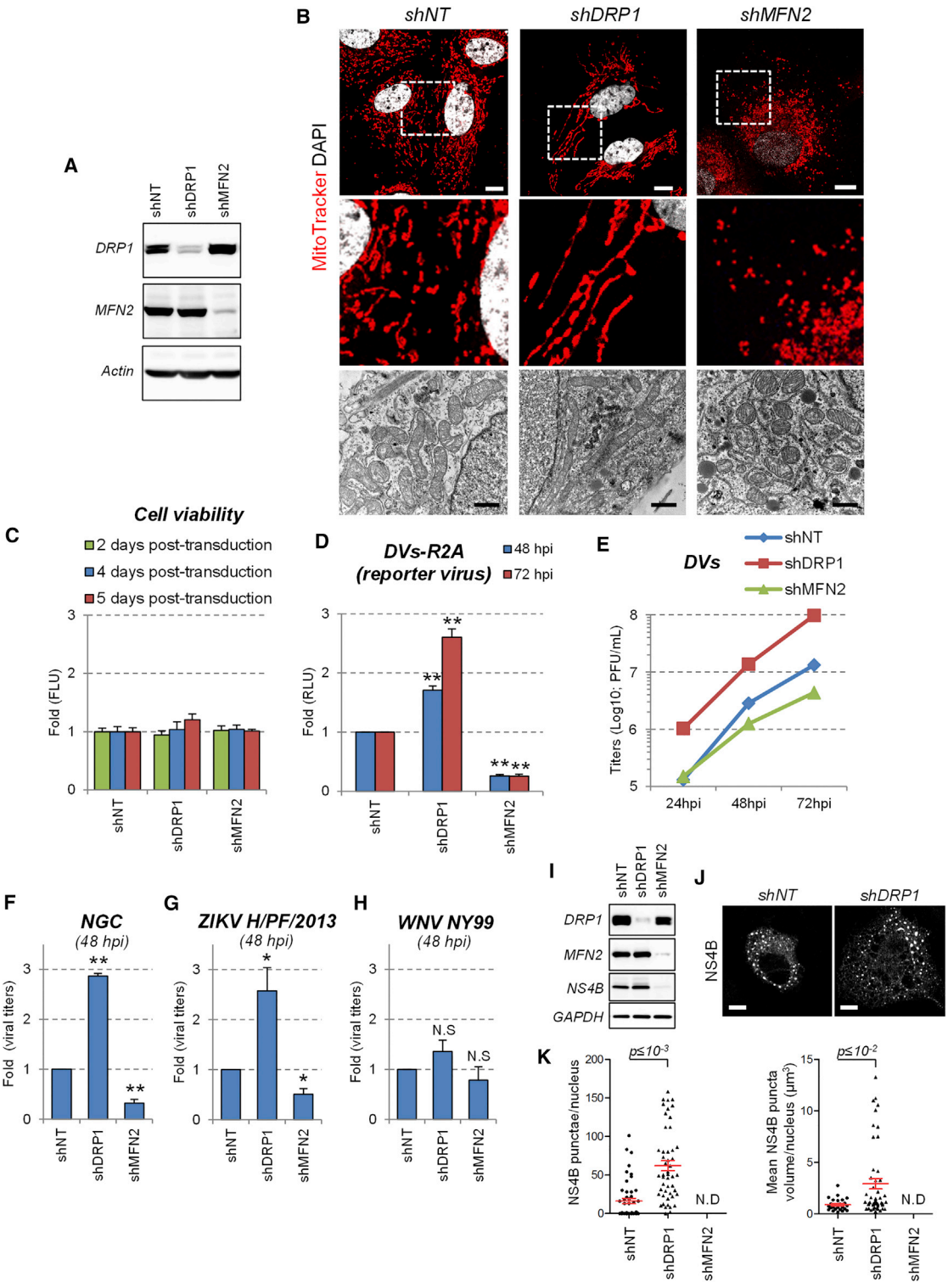

Figure 5. Mitochondria Elongation Favors DENV Replication

(A) Huh7 cells were transduced with shRNA-expressing lentiviruses. Four days post transduction, cells were collected and the expression of both DRP1 and MFN2 was analyzed by western blotting.

(B) The morphology of mitochondria in shRNA-transduced cells was analyzed by confocal microscopy after staining with MitoTracker or by TEM (lower panels). White scale bar, 10 μm; black scale bar, 1 μm.

(C) Cell viability of transduced cells was evaluated 2, 4, or 5 days post-transduction using the CellTiter-Glo assay, which is a measure for ATP levels in the cells.

(D–F) Two days post transduction, cells were infected with (D) the DVs-R2A reporter virus (MOI = 0.1), (E) DVs (MOI = 0.01), (F) NGC (MOI = 0.01).

(legend continued on next page)

and dampened IFN induction remain to be clarified, we propose that DENV NS4B induces mitochondria elongation to provide MAMs to NS4A, which stimulates CM biogenesis (Miller et al., 2007). Consequently, MAM-associated proteins, such as STING, would be hijacked and redirected to CMs. This accumulation of host factors in CMs may facilitate their cleavage by the NS2B-3 protease that is highly enriched in this compartment (Welsch et al., 2009). Whether such a DENV hijacking model could apply to additional MAM functions, such as autophagy, apoptosis, calcium transfer or ER-stress (van Vliet et al., 2014; Vance, 2014), remains to be determined.

Apart from NS4B-mediated alteration of DRP1 function, this or other DENV proteins might affect mitochondrial functions in alternative or perhaps complementary ways. For instance, our NS4B proteome identified many ATP synthase subunits, suggesting that DENV might alter local ATP production for the benefit of the biogenesis of membranous replication factories. Additionally, DENV might target VDAC2, also identified in our NS4B proteome and enriched in the MAMs, to perturb its functions in calcium homeostasis and apoptosis (Poston et al., 2013; Naghdi and Hajnoczky, 2016).

In conclusion, we provide compelling evidence for a mechanism of innate immunity interference by DENV that relies on virus-modulated morphodynamics of the mitochondria and their physical interactions with membranous viral replication factories. This subversion of innate immunity by DENV may have important implications for a better understanding of disease pathogenesis.

EXPERIMENTAL PROCEDURES

Further details of used experimental procedures are given in Supplemental Information.

Cell Lines and Virus Strains

Naive cell lines were cultured in DMEM (Life Technologies) containing 10% fetal bovine serum, 100 U/ml penicillin, 100 μg/ml streptomycin and 1% nonessential amino acids (complete DMEM). Production of virus stocks and determination of virus titers by plaque assays are specified in the Supplemental Information.

Live Cell Imaging

Huh7 reporter cells (2×10^5) were seeded into a 35-mm diameter glass bottom culture dish (MatTek). Cells were infected with a MOI of 10 for 1 hr at 37°C with occasional rocking. After removal of the inoculum, cells were washed thrice with PBS, and 2 ml phenol red-free DMEM (Life Technologies) containing 10% fetal calf serum was added. Image series of DENV-infected cells were acquired on a Nikon Eclipse Ti inverted microscope using a 40× Plan-Apo N.A. 0.95 objective (Nikon). Forty to 60 observation fields were defined, and image acquisition was performed at intervals of 1 hr for 72 hr by using the automated Nikon perfect focus system and CFP as well as YFP filters. Images were analyzed with the Nikon NIS Element Advanced Research program and processed by using the image processing package Fiji.

Transmission Electron Microscopy

Cells grown on glass coverslips were washed twice with pre-warmed PBS and fixed by 30 min incubation with 2.5% glutaraldehyde/2% sucrose in 50 mM sodium cacodylate buffer (CaCo) supplemented with 50 mM KCl, 2.6 mM MgCl2 and 2.6 mM CaCl2. After three washes with 50 mM CaCo, cells were incubated with 2% osmium tetroxide/50 mM CaCo for 40 min on ice, washed with water three times, and treated with 0.5% uranyl acetate for 30 min. After 30 min rinsing with water, cells were progressively dehydrated with increasing concentrations of ethanol (40% to 100%) and finally infiltrated in a polymerizing Epon/araldite resin (Araldite 502/Embed 812 kit; Electron Microscopy Sciences) for 72 hr at 60°C. Embedded cells were sectioned into 65-nm slices by using an Ultracut UCT microtome (Leica) and a diamond knife (Diatome). After counterstaining with 3% uranyl acetate in 70% methanol for 5 min and 2% lead citrate in water for 2 min, cells were examined with an EM-10 transmission electron microscope (Zeiss) with a built-in MegaView camera (Olympus). The length of mitochondria was measured using the ImageJ software package.

Correlative Light-Electron Microscopy

Huh7 cells stably expressing YFP-Sec61β and mito-mTurquoise2 were grown in 6-cm diameter dishes (Mattek) containing gridded coverslips and infected with DVs at a MOI of 1. Three days post infection, cells were washed twice and fixed by 20 min incubation with PBS containing 4% paraformaldehyde at room temperature. After several times washing with PBS, cells were examined with an Ultraview ERS spinning disc (PerkinElmer Life Sciences) on a Nikon TE2000-E inverted confocal microscope. Cells of interest were selected, and 0.13-μm optical sections in the cyan and YFP channels were acquired. The corresponding coordinates were also recorded using transmitted light with a differential interference contrast configuration. Cells were prepared and embedded for TEM analysis as previously described, and blocks were trimmed around the cell of interest according to the recorded coordinates. Ultrathin sections were prepared and examined with an EM-10 transmission electron microscope (Zeiss) containing a built-in MegaView camera (Olympus). Using ultrastructural and fluorescent patterns of mitochondria morphology and distribution, EM images and corresponding confocal microscopy Z-stacks were superimposed with the Photoshop CS5.1 software package (Adobe) and used for correlation analysis.

SUPPLEMENTAL INFORMATION

Supplemental Information includes Supplemental Experimental Procedures, seven figures, one table, and six movies and can be found with this article online at http://dx.doi.org/10.1016/j.chom.2016.07.008.

AUTHOR CONTRIBUTIONS

L.C.C. and R.B. designed the study. L.C.C. conducted most of the experiments. M.C. and I.R.B. have contributed equally to this work. M.C. prepared and imaged samples by TEM and CLEM. I.R.B. prepared the samples for FIB-SEM, which was conducted together with N.S. I.R.B. analyzed the FIB-SEM datasets and performed the 3D rendering. C.J.N. conducted subcellular fractionations. Y.S provided equipment and expertise for the FIB-SEM. S.B. and P.S. contributed to the analysis of the IFN response by real-time PCR. W.F. generated the NS4B-HA-expressing DVs and prepared the samples for

(G) ZIKV H/PF/2013 (MOI = 0.05) or (H) WNV NY99 (MOI = 0.05). At the indicated time points, Renilla luciferase activity (RLU) reflecting DENV RNA replication (D) or virus titers (E–H) were determined. Mean values and SD are indicated in (C) displaying a representative of at least three independent replicates. Mean values and SEM are indicated in (C) and (F)–(H) based on at least three independent experiments. $^{**}p \leq 10^{-3}$; $^{*}p \leq 10^{-2}$; N.S: not significant ($p \geq 0.05$).

(I) Huh7-T7 cells were transduced with shRNA-expressing lentiviruses and transfected three days post transduction with a plasmid encoding a DENV2 NS1-5 polyprotein. 16 hr later, cells were analyzed for knockdown efficiency and NS4B expression using western blotting.

(J) Cells from (I) were fixed, permeabilized and NS4B was visualized by immunofluorescence using confocal microscopy.

(K) Optical sections were acquired for 50 cells in two independent experiments and, after 3D reconstruction, number and mean volume of NS4B punctae per cell were determined.

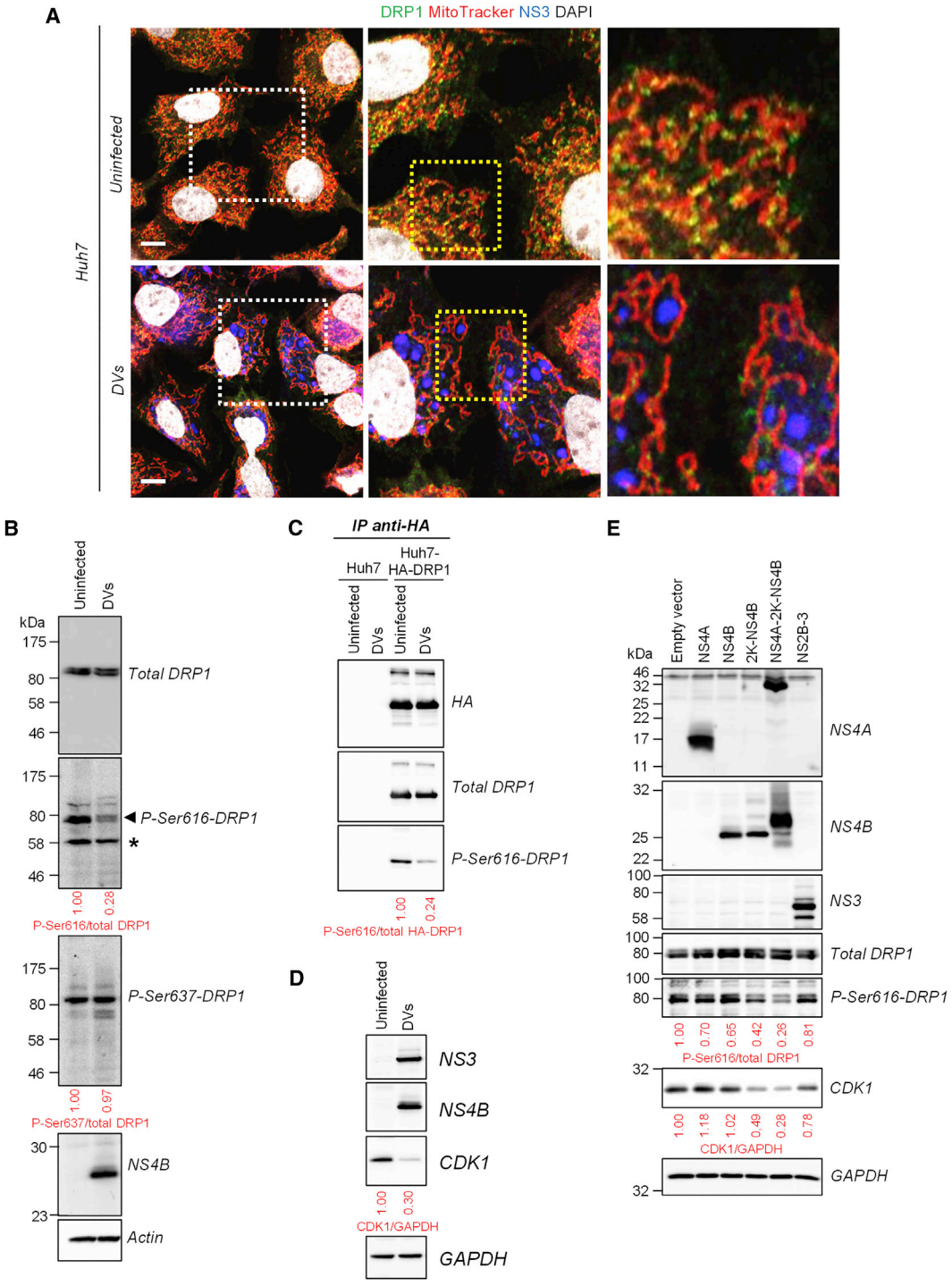

Figure 6. DENV2 Inhibits the Activation and Mitochondrial Translocation of the Fission Factor DRP1

(A) Huh7 cells were infected with DVs (MOI = 1). Three days post infection, cells were labeled with MitoTracker, DAPI and antibodies specified on the top. Dotted boxes indicate areas that are enlarged in the respective adjacent panel. Scale bar, 10 μm.

(B) Extracts of naive or DVs-infected cells were prepared 72 hr after infection and analyzed by western blotting using antibodies recognizing differentially phosphorylated (Ser616 or Ser637) or total DRP1. *Non-specific band.

(C) Extracts of Huh7 and HA-DRP1-overexpressing Huh7 cells were subjected to immunoprecipitation using an HA-specific antibody. Captured complexes were analyzed by western blotting for phosphorylated and total DRP1.

(D) Cell lysates were prepared as in (B) and analyzed by western blotting.

(E) Huh7 cells were transduced with lentiviruses expressing the indicated DENV proteins (MOI = 5). Four days later, cell extracts were prepared and analyzed for the expression of the indicated proteins using western blotting.

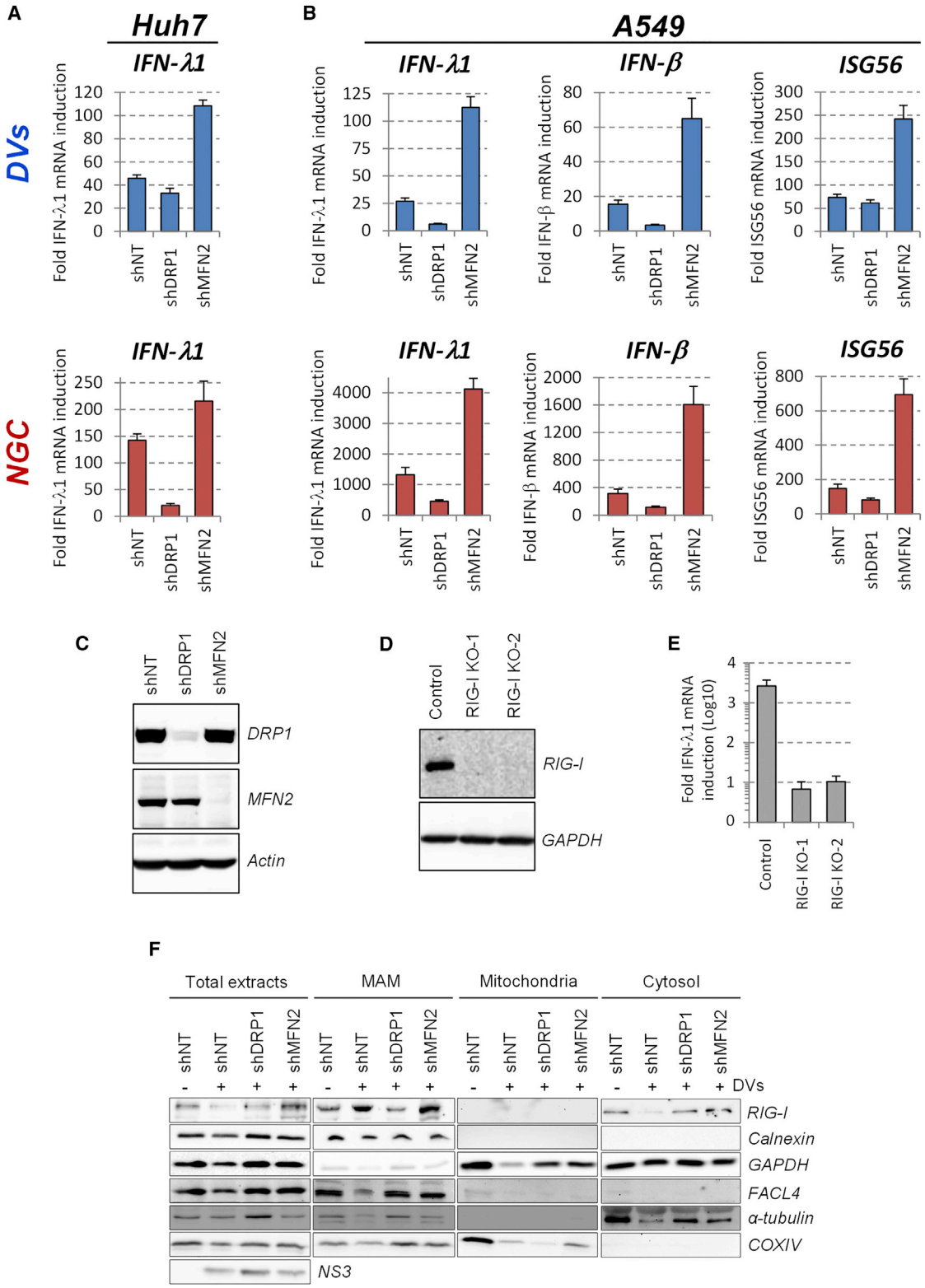

Figure 7. Mitochondria Elongation Alleviates DENV2-Induced Activation of the Interferon Response

Huh7 and A549 cells were transduced with DRP1- or MFN2-specific shRNA-encoding lentiviruses. Two (Huh7) or three (A549) days post-transduction, cells were infected with DENV2 DVs or NGC (MOI = 5).

(A and B) 48 (Huh7) or 24 (A549) hr later, cells were collected and mRNA amounts of IFN-λ1, IFN-β, and ISG56 were quantified using qRT-PCR. Quantifications are representative of three independent replicates.

(legend continued on next page)

quantitative mass spectrometry analysis, which was evaluated by B.F. A.R. performed live-cell imaging. L.C.C. and R.B. wrote the manuscript. R.B. supervised the study.

ACKNOWLEDGMENTS

We are grateful to Dr. Vibor Laketa and the Infectious Diseases Imaging Platform (IDIP) at the Department of Infectious Diseases, University Hospital Heidelberg, for providing excellent microscopy support. We acknowledge Progen Biotechnik GmbH, Heidelberg for providing DENV serotypes 1, 3, and 4; Andrew Davidson for the NGC strain; Jonas Schmidt-Chanasit for the WNV NY99 strain; and the European Virus Archive for ZIKV strains. We thank Uta Haselmann, Marie Bartenschlager, Ulrike Herian, and Jacomine Krijnse-Locker for technical help; Dr. Didier Trono for lentivirus packaging constructs; Dr. Nathan R. Brady for DRP1 cDNA; Dr. Gualtiero Alvisi for constructing the YFP-Sec61β-encoding plasmid; and Drs. Eliana G. Acosta, Anil Kumar, David Paul, and Philippe Metz for virus stock production. We thank Dr. Birgit Voigt, proteomics platform of the Institute of Microbiology, University of Greifswald, for mass spectrometry-based analysis of the DENV NS4B interactome. We are grateful to the Electron Microscopy Core Facility of the University of Heidelberg and at the EMBL for expert support and providing access to their equipment. This work was supported by grants from the Deutsche Forschungsgemeinschaft (SFB 638, TP A5, and SFB 1129, TP11) to R.B. and SFB 1129 (TP13) to A.R.

Received: February 23, 2016
Revised: June 21, 2016
Accepted: July 22, 2016
Published: August 18, 2016

REFERENCES

Acosta, E.G., Kumar, A., and Bartenschlager, R. (2014). Revisiting dengue virus-host cell interaction: new insights into molecular and cellular virology. Adv. Virus Res. *88*, 1–109.

Aguirre, S., Maestre, A.M., Pagni, S., Patel, J.R., Savage, T., Gutman, D., Maringer, K., Bernal-Rubio, D., Shabman, R.S., Simon, V., et al. (2012). DENV inhibits type I IFN production in infected cells by cleaving human STING. PLoS Pathog. *8*, e1002934.

Bhatt, S., Gething, P.W., Brady, O.J., Messina, J.P., Farlow, A.W., Moyes, C.L., Drake, J.M., Brownstein, J.S., Hoen, A.G., Sankoh, O., et al. (2013). The global distribution and burden of dengue. Nature *496*, 504–507.

Castanier, C., Garcin, D., Vazquez, A., and Arnoult, D. (2010). Mitochondrial dynamics regulate the RIG-I-like receptor antiviral pathway. EMBO Rep. *11*, 133–138.

Chan, D.C. (2012). Fusion and fission: interlinked processes critical for mitochondrial health. Annu. Rev. Genet. *46*, 265–287.

Chan, Y.K., and Gack, M.U. (2016). A phosphomimetic-based mechanism of dengue virus to antagonize innate immunity. Nat. Immunol. *17*, 523–530.

Chatel-Chaix, L., and Bartenschlager, R. (2014). Dengue virus- and hepatitis C virus-induced replication and assembly compartments: the enemy inside–caught in the web. J. Virol. *88*, 5907–5911.

Chatel-Chaix, L., Fischl, W., Scaturro, P., Cortese, M., Kallis, S., Bartenschlager, M., Fischer, B., and Bartenschlager, R. (2015). A Combined Genetic-Proteomic Approach Identifies Residues within Dengue Virus NS4B Critical for Interaction with NS3 and Viral Replication. J. Virol. *89*, 7170–7186.

Chen, Y., and Dorn, G.W., 2nd (2013). PINK1-phosphorylated mitofusin 2 is a Parkin receptor for culling damaged mitochondria. Science *340*, 471–475.

Chen, H., Detmer, S.A., Ewald, A.J., Griffin, E.E., Fraser, S.E., and Chan, D.C. (2003). Mitofusins Mfn1 and Mfn2 coordinately regulate mitochondrial fusion and are essential for embryonic development. J. Cell Biol. *160*, 189–200.

Dalrymple, N.A., Cimica, V., and Mackow, E.R. (2015). Dengue Virus NS Proteins Inhibit RIG-I/MAVS Signaling by Blocking TBK1/IRF3 Phosphorylation: Dengue Virus Serotype 1 NS4A Is a Unique Interferon-Regulating Virulence Determinant. MBio *6*, e00553–15.

Friedman, J.R., Lackner, L.L., West, M., DiBenedetto, J.R., Nunnari, J., and Voeltz, G.K. (2011). ER tubules mark sites of mitochondrial division. Science *334*, 358–362.

Glauser, L., Sonnay, S., Stafa, K., and Moore, D.J. (2011). Parkin promotes the ubiquitination and degradation of the mitochondrial fusion factor mitofusin 1. J. Neurochem. *118*, 636–645.

Horner, S.M., Liu, H.M., Park, H.S., Briley, J., and Gale, M., Jr. (2011). Mitochondrial-associated endoplasmic reticulum membranes (MAM) form innate immune synapses and are targeted by hepatitis C virus. Proc. Natl. Acad. Sci. USA *108*, 14590–14595.

Kakumani, P.K., Ponia, S.S., Rajgokul, K.S., Sood, V., Chinnappan, M., Banerjea, A.C., Medigeshi, G.R., Malhotra, P., Mukherjee, S.K., and Bhatnagar, R.K. (2013). Role of RNA interference (RNAi) in dengue virus replication and identification of NS4B as an RNAi suppressor. J. Virol. *87*, 8870–8883.

Kim, S.J., Syed, G.H., Khan, M., Chiu, W.W., Sohail, M.A., Gish, R.G., and Siddiqui, A. (2014). Hepatitis C virus triggers mitochondrial fission and attenuates apoptosis to promote viral persistence. Proc. Natl. Acad. Sci. USA *111*, 6413–6418.

Knoops, K., Kikkert, M., Worm, S.H., Zevenhoven-Dobbe, J.C., van der Meer, Y., Koster, A.J., Mommaas, A.M., and Snijder, E.J. (2008). SARS-coronavirus replication is supported by a reticulovesicular network of modified endoplasmic reticulum. PLoS Biol. *6*, e226.

Korobova, F., Ramabhadran, V., and Higgs, H.N. (2013). An actin-dependent step in mitochondrial fission mediated by the ER-associated formin INF2. Science *339*, 464–467.

Leboucher, G.P., Tsai, Y.C., Yang, M., Shaw, K.C., Zhou, M., Veenstra, T.D., Glickman, M.H., and Weissman, A.M. (2012). Stress-induced phosphorylation and proteasomal degradation of mitofusin 2 facilitates mitochondrial fragmentation and apoptosis. Mol. Cell *47*, 547–557.

Lee, H., and Yoon, Y. (2014). Mitochondrial fission: regulation and ER connection. Mol. Cells *37*, 89–94.

Manor, U., Bartholomew, S., Golani, G., Christenson, E., Kozlov, M., Higgs, H., Spudich, J., and Lippincott-Schwartz, J. (2015). A mitochondria-anchored isoform of the actin-nucleating spire protein regulates mitochondrial division. eLife *4*, e08828.

McLean, J.E., Wudzinska, A., Datan, E., Quaglino, D., and Zakeri, Z. (2011). Flavivirus NS4A-induced autophagy protects cells against death and enhances virus replication. J. Biol. Chem. *286*, 22147–22159.

Miller, S., Kastner, S., Krijnse-Locker, J., Bühler, S., and Bartenschlager, R. (2007). The non-structural protein 4A of dengue virus is an integral membrane

(C) Knockdown efficiency in A549 cells was monitored 4 days post transduction by western blotting using MFN2- and DRP1-specific antibodies. Actin served as loading control.

(D) Huh7 RIG-I knockout cell pools were generated by CRISPR/Cas9 technology using two different guide RNAs and lysates of cells were analyzed by western blotting.

(E) RIG-I knockout cells were infected with DVs or left uninfected. Two days later, abundance of IFN-λ1 and β-actin mRNA was measured using qRT-PCR. IFN-λ1 induction levels upon infection were calculated after normalization to β-actin. For qRT-PCR experiments (A, B, E), error bars indicate SD calculated using three technical replicates.

(F) Huh7 cells were transduced and infected with DVs as in (A). Cell extracts were subjected to subcellular fractionation to isolate MAMs. Equal amounts of proteins from each fraction were analyzed by western blotting using antibodies recognizing the indicated proteins. FACL4 and calnexin served as markers enriched in the MAM fraction and α-tubulin as cytosolic marker.

protein inducing membrane alterations in a 2K-regulated manner. J. Biol. Chem. *282*, 8873–8882.

Muñoz-Jordan, J.L., Sánchez-Burgos, G.G., Laurent-Rolle, M., and García-Sastre, A. (2003). Inhibition of interferon signaling by dengue virus. Proc. Natl. Acad. Sci. USA *100*, 14333–14338.

Muñoz-Jordán, J.L., Laurent-Rolle, M., Ashour, J., Martínez-Sobrido, L., Ashok, M., Lipkin, W.I., and García-Sastre, A. (2005). Inhibition of alpha/beta interferon signaling by the NS4B protein of flaviviruses. J. Virol. *79*, 8004–8013.

Naghdi, S., and Hajnoczky, G. (2016). VDAC2-specific cellular functions and the underlying structure. Biochim. Biophys. Acta., Published online April 23, 2016. http://dx.doi.org/10.1016/j.bbamcr.2016.04.020.

Olichon, A., Baricault, L., Gas, N., Guillou, E., Valette, A., Belenguer, P., and Lenaers, G. (2003). Loss of OPA1 perturbates the mitochondrial inner membrane structure and integrity, leading to cytochrome c release and apoptosis. J. Biol. Chem. *278*, 7743–7746.

Onoguchi, K., Onomoto, K., Takamatsu, S., Jogi, M., Takemura, A., Morimoto, S., Julkunen, I., Namiki, H., Yoneyama, M., and Fujita, T. (2010). Virus-infection or 5'ppp-RNA activates antiviral signal through redistribution of IPS-1 mediated by MFN1. PLoS Pathog. *6*, e1001012.

Otera, H., Wang, C., Cleland, M.M., Setoguchi, K., Yokota, S., Youle, R.J., and Mihara, K. (2010). Mff is an essential factor for mitochondrial recruitment of Drp1 during mitochondrial fission in mammalian cells. J. Cell Biol. *191*, 1141–1158.

Paul, D., and Bartenschlager, R. (2013). Architecture and biogenesis of plus-strand RNA virus replication factories. World J. Virol. *2*, 32–48.

Poston, C.N., Krishnan, S.C., and Bazemore-Walker, C.R. (2013). In-depth proteomic analysis of mammalian mitochondria-associated membranes (MAM). J. Proteomics *79*, 219–230.

Pyakurel, A., Savoia, C., Hess, D., and Scorrano, L. (2015). Extracellular regulated kinase phosphorylates mitofusin 1 to control mitochondrial morphology and apoptosis. Mol. Cell *58*, 244–254.

Shi, C.S., Qi, H.Y., Boularan, C., Huang, N.N., Abu-Asab, M., Shelhamer, J.H., and Kehrl, J.H. (2014). SARS-coronavirus open reading frame-9b suppresses innate immunity by targeting mitochondria and the MAVS/TRAF3/TRAF6 signalosome. J. Immunol. *193*, 3080–3089.

Smirnova, E., Shurland, D.L., Ryazantsev, S.N., and van der Bliek, A.M. (1998). A human dynamin-related protein controls the distribution of mitochondria. J. Cell Biol. *143*, 351–358.

Smirnova, E., Griparic, L., Shurland, D.L., and van der Bliek, A.M. (2001). Dynamin-related protein Drp1 is required for mitochondrial division in mammalian cells. Mol. Biol. Cell *12*, 2245–2256.

Strack, S., and Cribbs, J.T. (2012). Allosteric modulation of Drp1 mechanoenzyme assembly and mitochondrial fission by the variable domain. J. Biol. Chem. *287*, 10990–11001.

Sun, L., Xing, Y., Chen, X., Zheng, Y., Yang, Y., Nichols, D.B., Clementz, M.A., Banach, B.S., Li, K., Baker, S.C., and Chen, Z. (2012). Coronavirus papain-like proteases negatively regulate antiviral innate immune response through disruption of STING-mediated signaling. PLoS ONE *7*, e30802.

van Vliet, A.R., Verfaillie, T., and Agostinis, P. (2014). New functions of mitochondria associated membranes in cellular signaling. Biochim. Biophys. Acta *1843*, 2253–2262.

Vance, J.E. (2014). MAM (mitochondria-associated membranes) in mammalian cells: lipids and beyond. Biochim. Biophys. Acta *1841*, 595–609.

Welsch, S., Miller, S., Romero-Brey, I., Merz, A., Bleck, C.K., Walther, P., Fuller, S.D., Antony, C., Krijnse-Locker, J., and Bartenschlager, R. (2009). Composition and three-dimensional architecture of the dengue virus replication and assembly sites. Cell Host Microbe *5*, 365–375.

Westaway, E.G., Mackenzie, J.M., Kenney, M.T., Jones, M.K., and Khromykh, A.A. (1997). Ultrastructure of Kunjin virus-infected cells: colocalization of NS1 and NS3 with double-stranded RNA, and of NS2B with NS3, in virus-induced membrane structures. J. Virol. *71*, 6650–6661.

World Health Organization. (2009). Dengue: Guidelines for Diagnosis,Treatment, Prevention and Control (World Health Organization).

Xia, M., Gonzalez, P., Li, C., Meng, G., Jiang, A., Wang, H., Gao, Q., Debatin, K.M., Beltinger, C., and Wei, J. (2014). Mitophagy enhances oncolytic measles virus replication by mitigating DDX58/RIG-I-like receptor signaling. J. Virol. *88*, 5152–5164.

Xie, X., Zou, J., Wang, Q.Y., and Shi, P.Y. (2015). Targeting dengue virus NS4B protein for drug discovery. Antiviral Res. *118*, 39–45.

Yasukawa, K., Oshiumi, H., Takeda, M., Ishihara, N., Yanagi, Y., Seya, T., Kawabata, S., and Koshiba, T. (2009). Mitofusin 2 inhibits mitochondrial antiviral signaling. Sci. Signal. *2*, ra47.

Yoshizumi, T., Ichinohe, T., Sasaki, O., Otera, H., Kawabata, S., Mihara, K., and Koshiba, T. (2014). Influenza A virus protein PB1-F2 translocates into mitochondria via Tom40 channels and impairs innate immunity. Nat. Commun. *5*, 4713.

Yu, C.Y., Chang, T.H., Liang, J.J., Chiang, R.L., Lee, Y.L., Liao, C.L., and Lin, Y.L. (2012). Dengue virus targets the adaptor protein MITA to subvert host innate immunity. PLoS Pathog. *8*, e1002780.

Yu, C.Y., Liang, J.J., Li, J.K., Lee, Y.L., Chang, B.L., Su, C.I., Huang, W.J., Lai, M.M., and Lin, Y.L. (2015). Dengue Virus Impairs Mitochondrial Fusion by Cleaving Mitofusins. PLoS Pathog. *11*, e1005350.

Ziviani, E., Tao, R.N., and Whitworth, A.J. (2010). Drosophila parkin requires PINK1 for mitochondrial translocation and ubiquitinates mitofusin. Proc. Natl. Acad. Sci. USA *107*, 5018–5023.

Cell Host & Microbe, Volume *20*

Supplemental Information

Dengue Virus Perturbs Mitochondrial Morphodynamics to Dampen Innate Immune Responses

Laurent Chatel-Chaix, Mirko Cortese, Inés Romero-Brey, Silke Bender, Christopher John Neufeldt, Wolfgang Fischl, Pietro Scaturro, Nicole Schieber, Yannick Schwab, Bernd Fischer, Alessia Ruggieri, and Ralf Bartenschlager

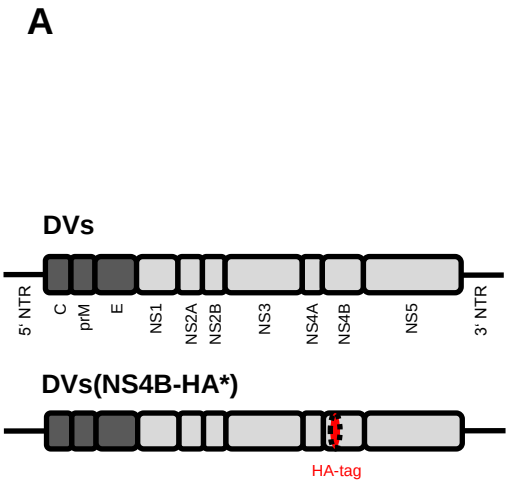

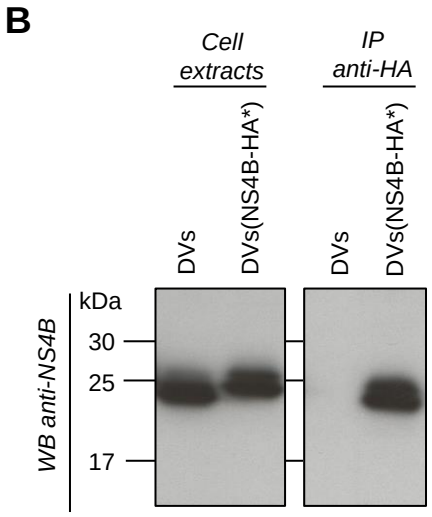

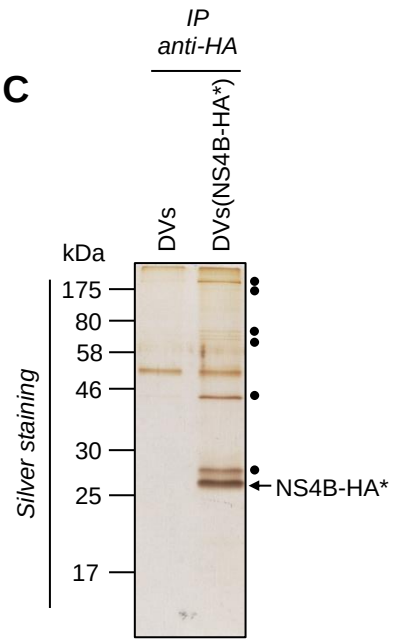

D

Name	ENSEMBL ID	Log2 Fold Enrichment	p-value
ATP5A1	ENSG00000152234	4.30	2.01E-07
ATP5B	ENSG00000110955	3.59	2.52E-07
CANX	ENSG00000127022	4.87	1.41E-05
GHITM	ENSG00000165678	Infinite	1.79E-04
SLC3A2	ENSG00000168003	Infinite	4.03E-04
ATP2A2	ENSG00000174437	Infinite	1.58E-03
ATP5O	ENSG00000241837	3.58	3.10E-03
HM13	ENSG00000101294	Infinite	4.40E-03
ATP5H	ENSG00000167863	Infinite	7.60E-03
VDAC2	ENSG00000165637	3.57	8.47E-03
ATP1A1	ENSG00000163399	Infinite	1.12E-02
APOB	ENSG00000084674	4.49	1.40E-02
IMMT	ENSG00000132305	Infinite	2.32E-02
MAOB	ENSG00000069535	Infinite	2.56E-02
HSPD1	ENSG00000144381	2.97	2.57E-02
ATP5C1	ENSG00000165629	3.67	3.21E-02
BAG2	ENSG00000112208	3.58	3.38E-02
ATP5F1	ENSG00000116459	3.38	4.52E-02
CHCHD3	ENSG00000106554	Infinite	4.79E-02

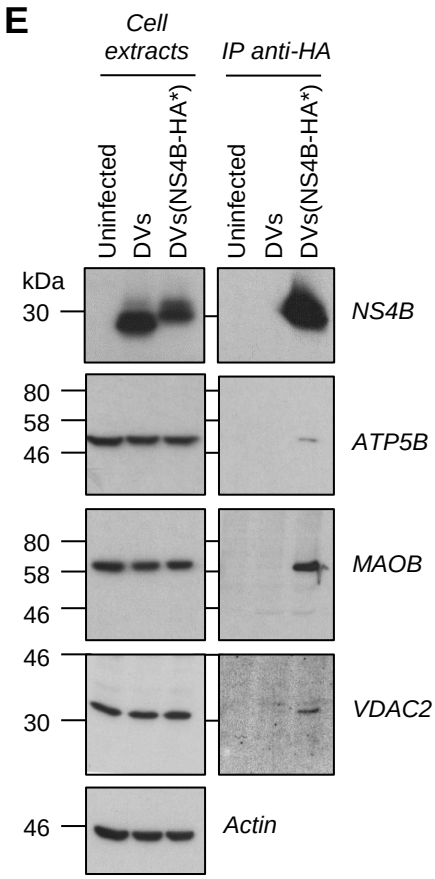

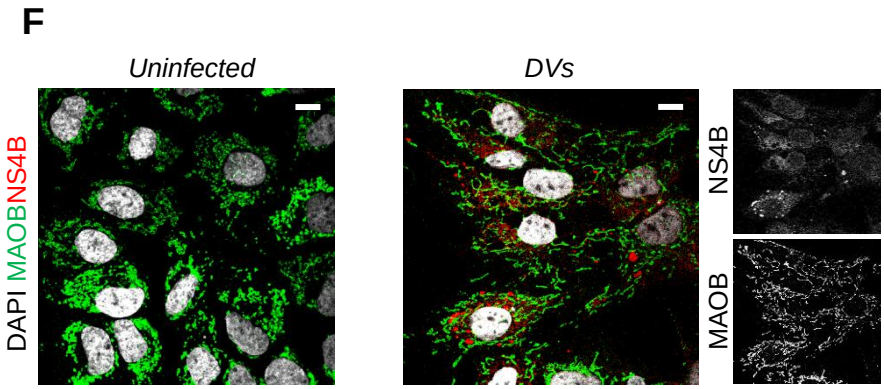

Figure S1

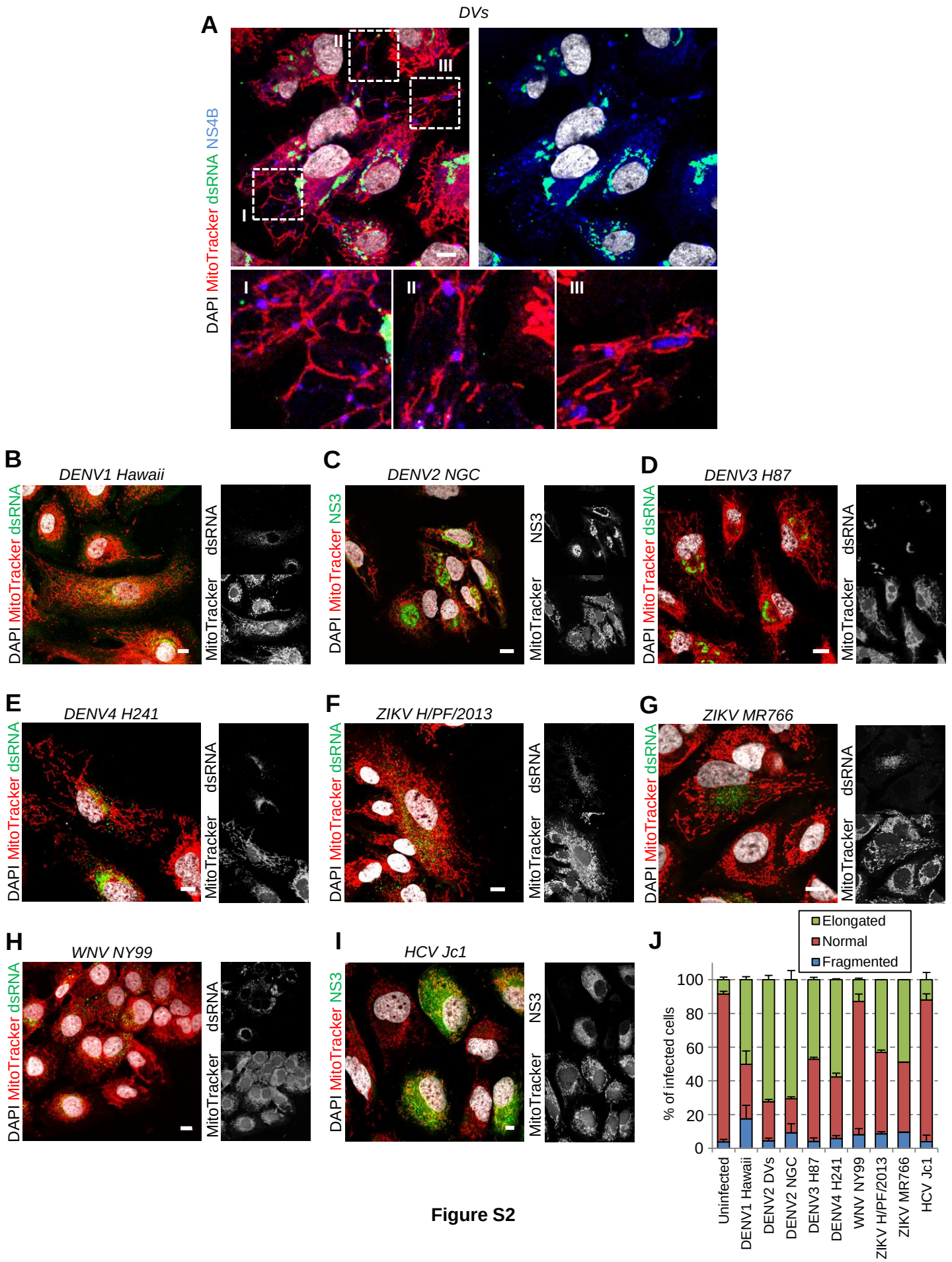
A
DVs
DAPI MitoTracker dsRNA NS4B
I
II
III
B
DENV1 Hawaii
C
DENV2 NGC
D
DENV3 H87
E
DENV4 H241
F
ZIKV H/PF/2013
G
ZIKV MR766
H
WNV NY99
I
HCV Jc1
DAPI MitoTracker dsRNA
MitoTracker dsRNA
DAPI MitoTracker NS3
MitoTracker NS3
J
Elongated
Normal
Fragmented
% of infected cells
0
20
40
60
80
100
Uninfected
DENV1 Hawaii
DENV2 DVs
DENV2 NGC
DENV3 H87
DENV4 H241
WNV NY99
ZIKV H/PF/2013
ZIKV MR766
HCV Jc1

Figure S2

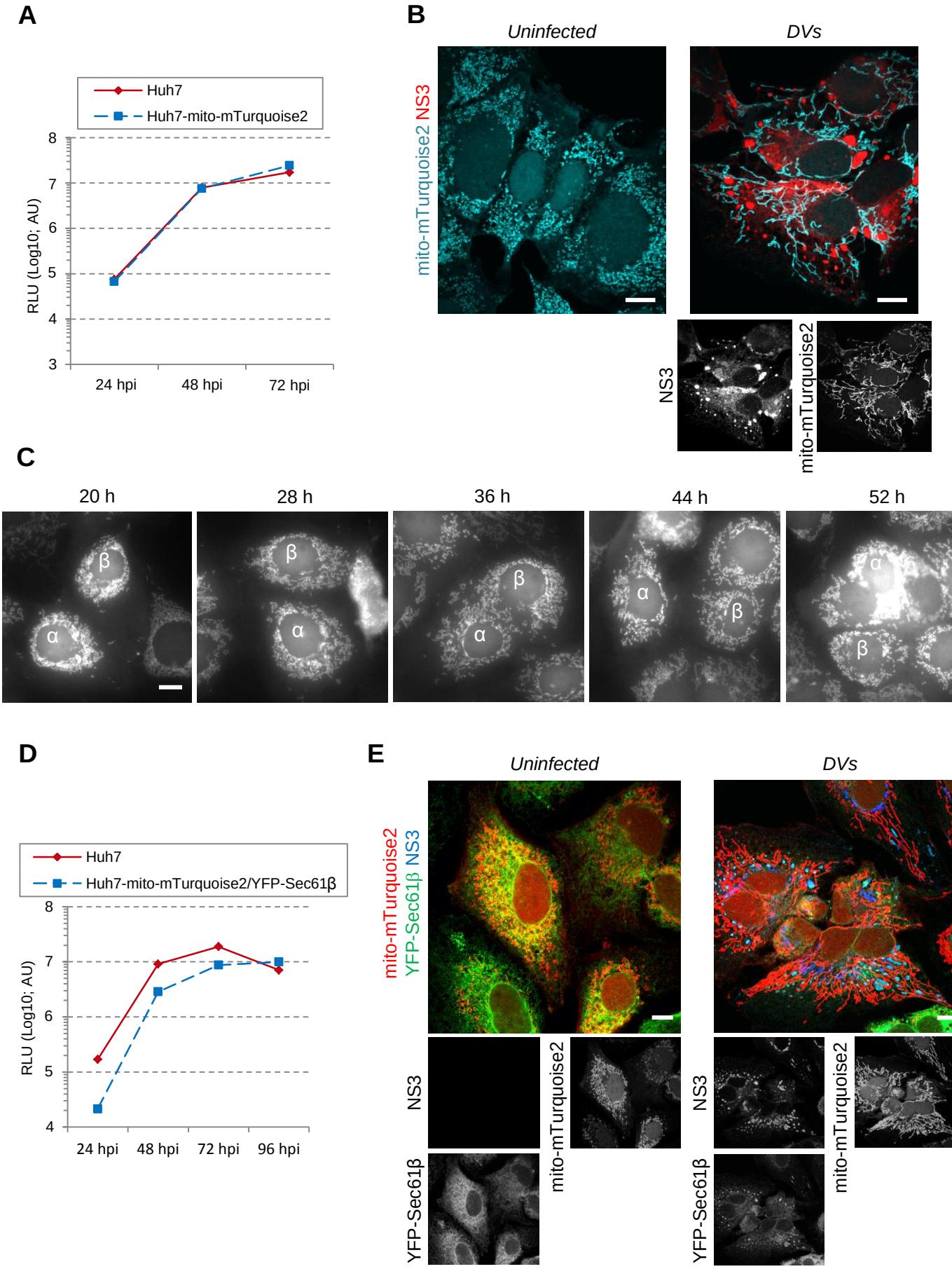
A
Huh7
Huh7-mito-mTurquoise2
RLU (Log10; AU)
8
7
6
5
4
3
24 hpi
48 hpi
72 hpi
B
Uninfected
DVs
mito-mTurquoise2 NS3
NS3
mito-mTurquoise2
C
20 h
28 h
36 h
44 h
52 h
Uninfected
β
α
D
Huh7
Huh7-mito-mTurquoise2/YFP-Sec61β
RLU (Log10; AU)
8
7
6
5
4
24 hpi
48 hpi
72 hpi
96 hpi
E
Uninfected
DVs
mito-mTurquoise2
YFP-Sec61β NS3
NS3
mito-mTurquoise2
YFP-Sec61β

Figure S3

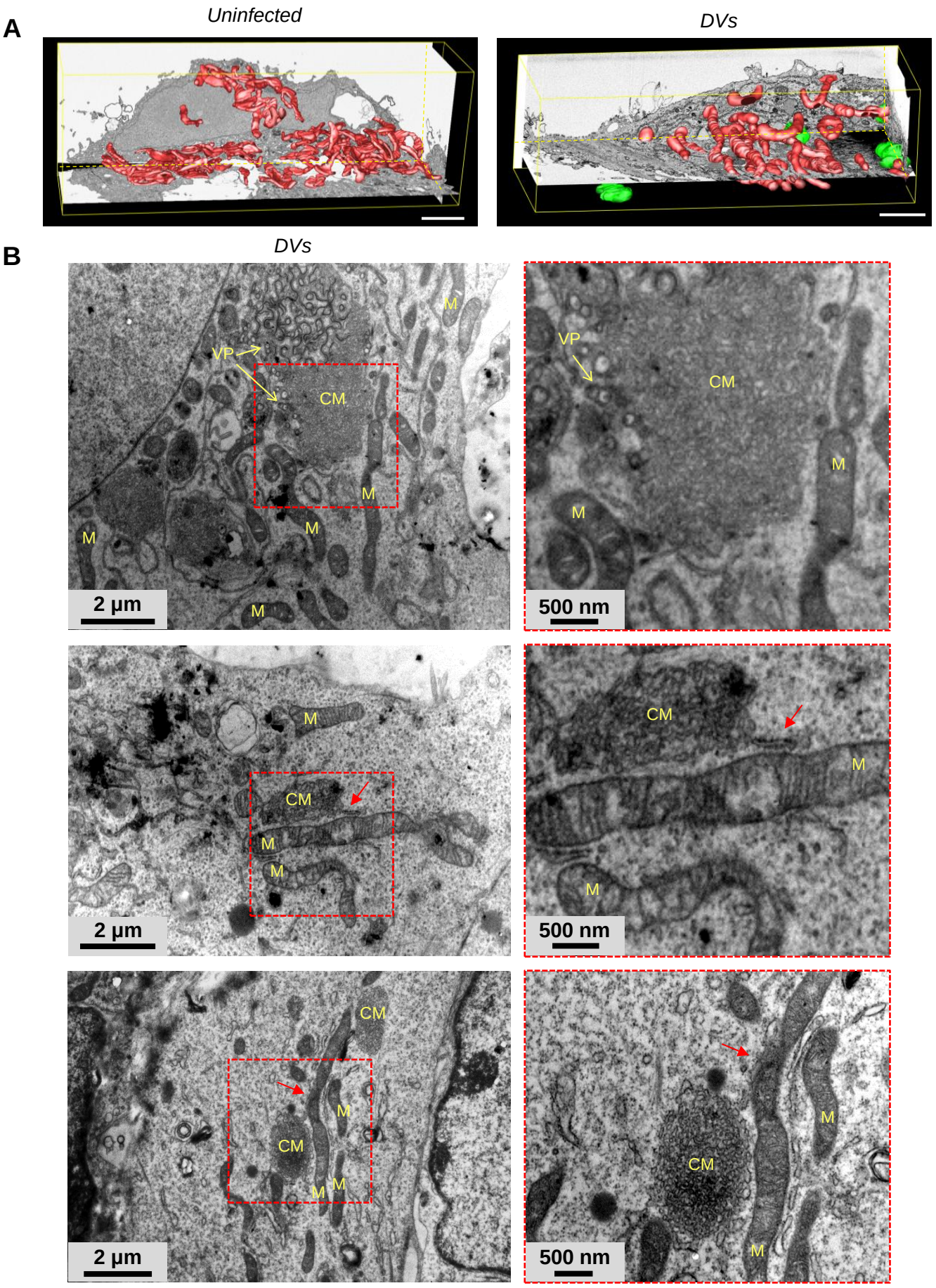

Figure S4

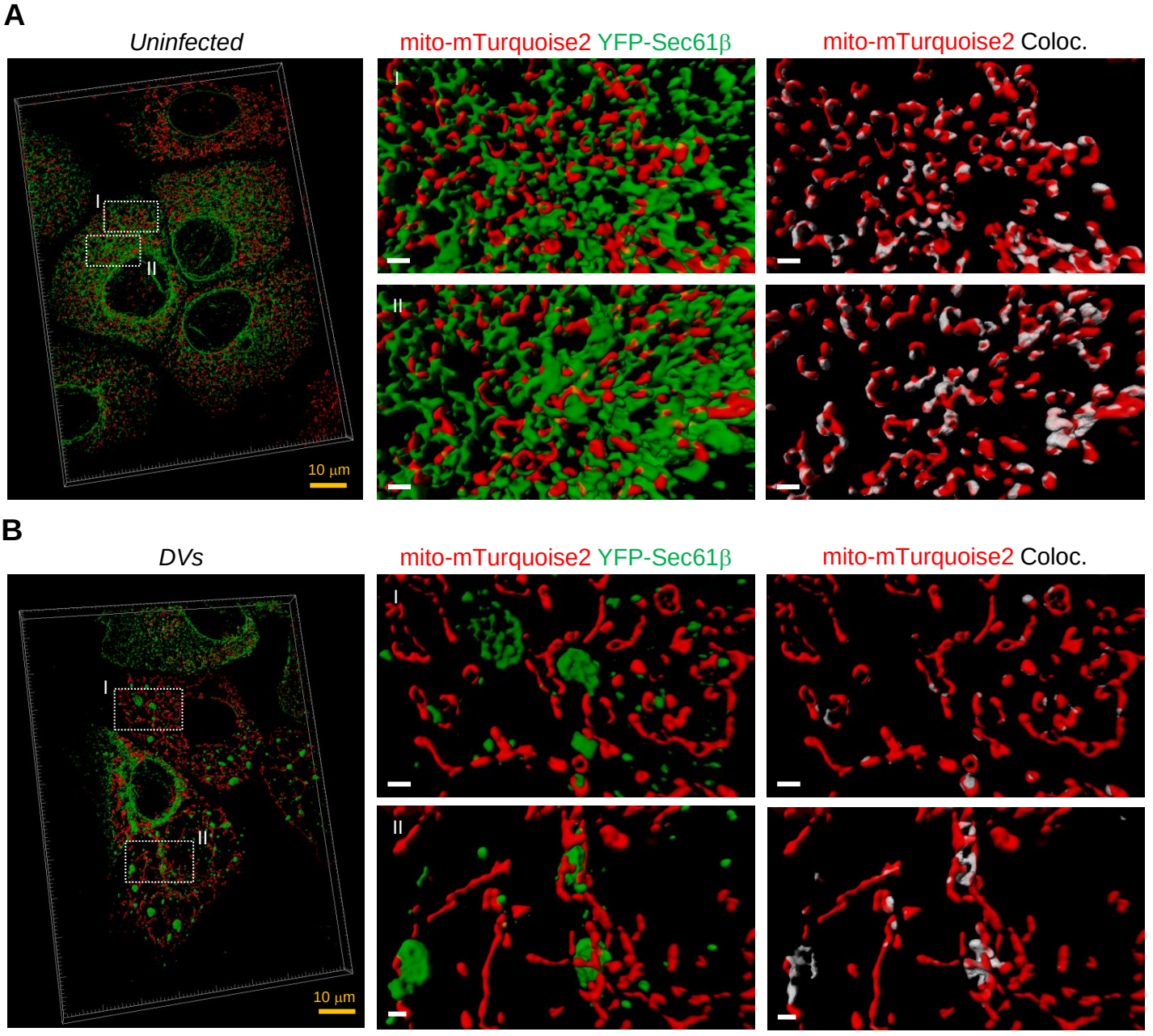
A
Uninfected
mito-mTurquoise2 YFP-Sec61β
mito-mTurquoise2 Coloc.
I
II
10 μm
B
DVs
mito-mTurquoise2 YFP-Sec61β
mito-mTurquoise2 Coloc.
I
II
10 μm

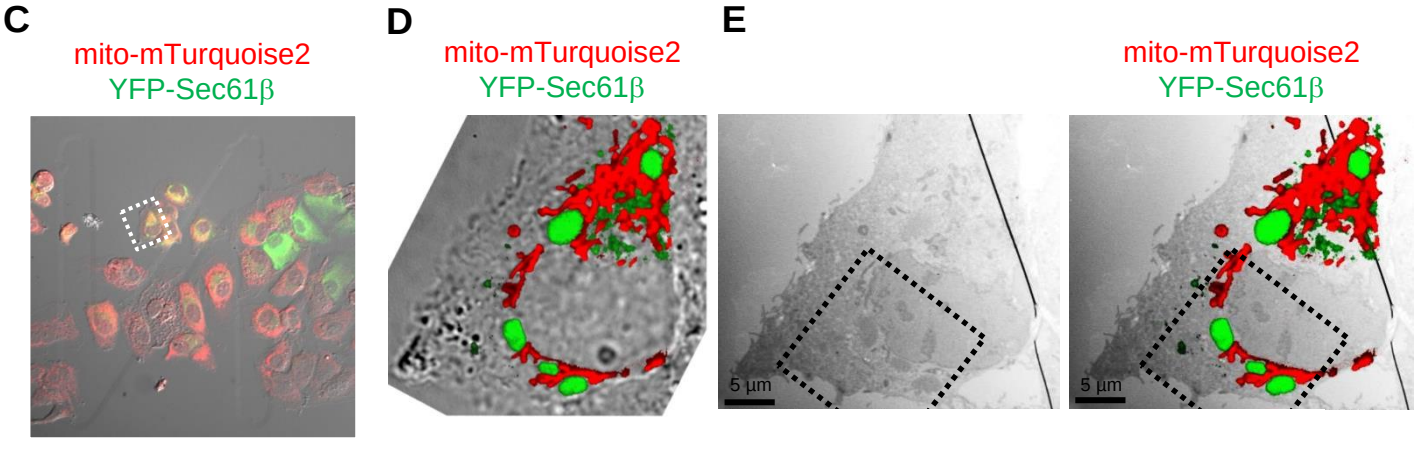
C
mito-mTurquoise2
YFP-Sec61β
D
mito-mTurquoise2
YFP-Sec61β
E
mito-mTurquoise2
YFP-Sec61β
5 μm
5 μm

Figure S5

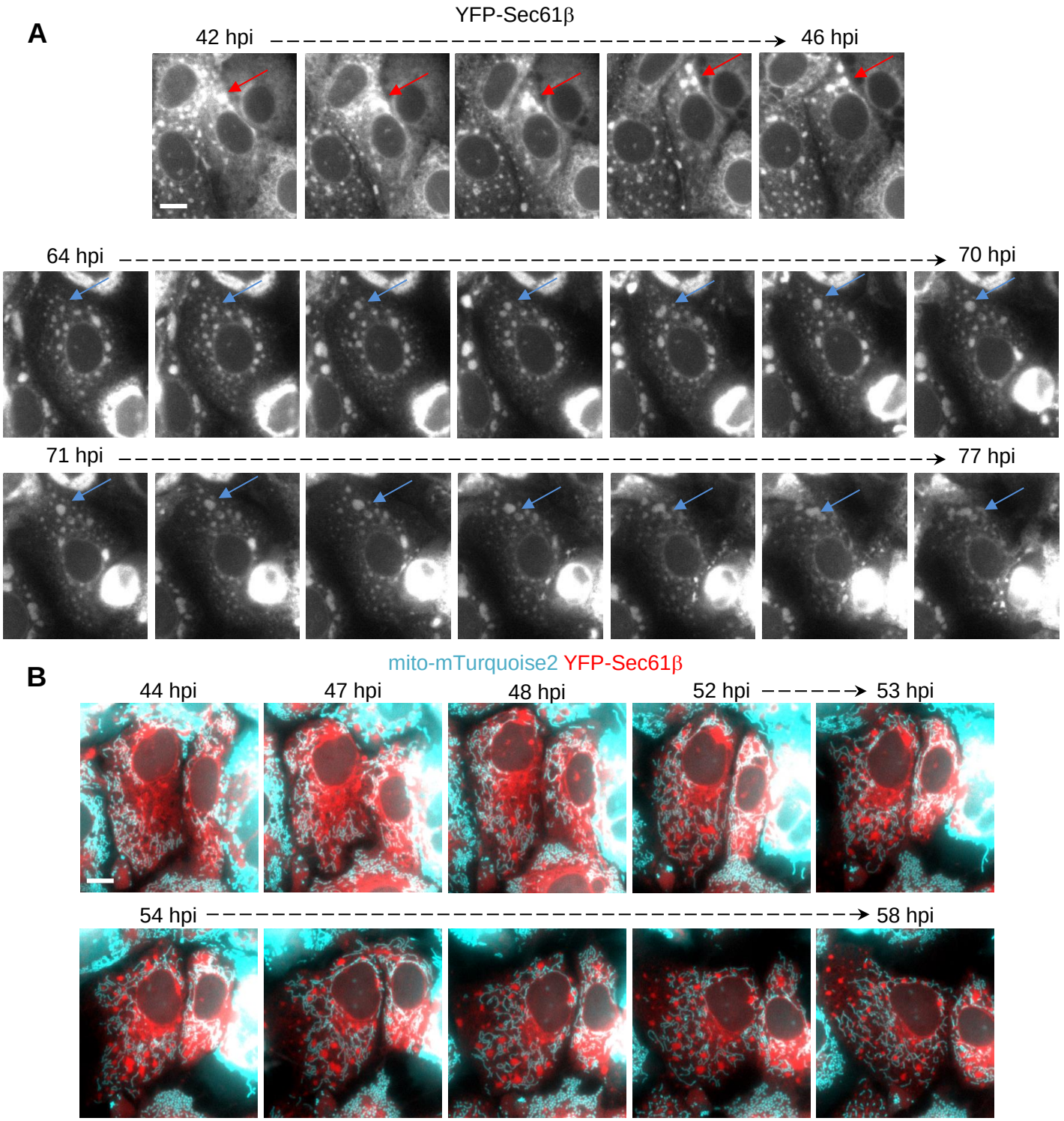
A
YFP-Sec61β
42 hpi
46 hpi
64 hpi
70 hpi
71 hpi
77 hpi
B
mito-mTurquoise2 YFP-Sec61β
44 hpi
47 hpi
48 hpi
52 hpi
53 hpi
54 hpi
58 hpi
C
ZIKV MR766
Fold (viral titers)
shNT
shDRP1
HCV JcR2A
Fold (RLU)
shNT
shDRP1

Figure S6

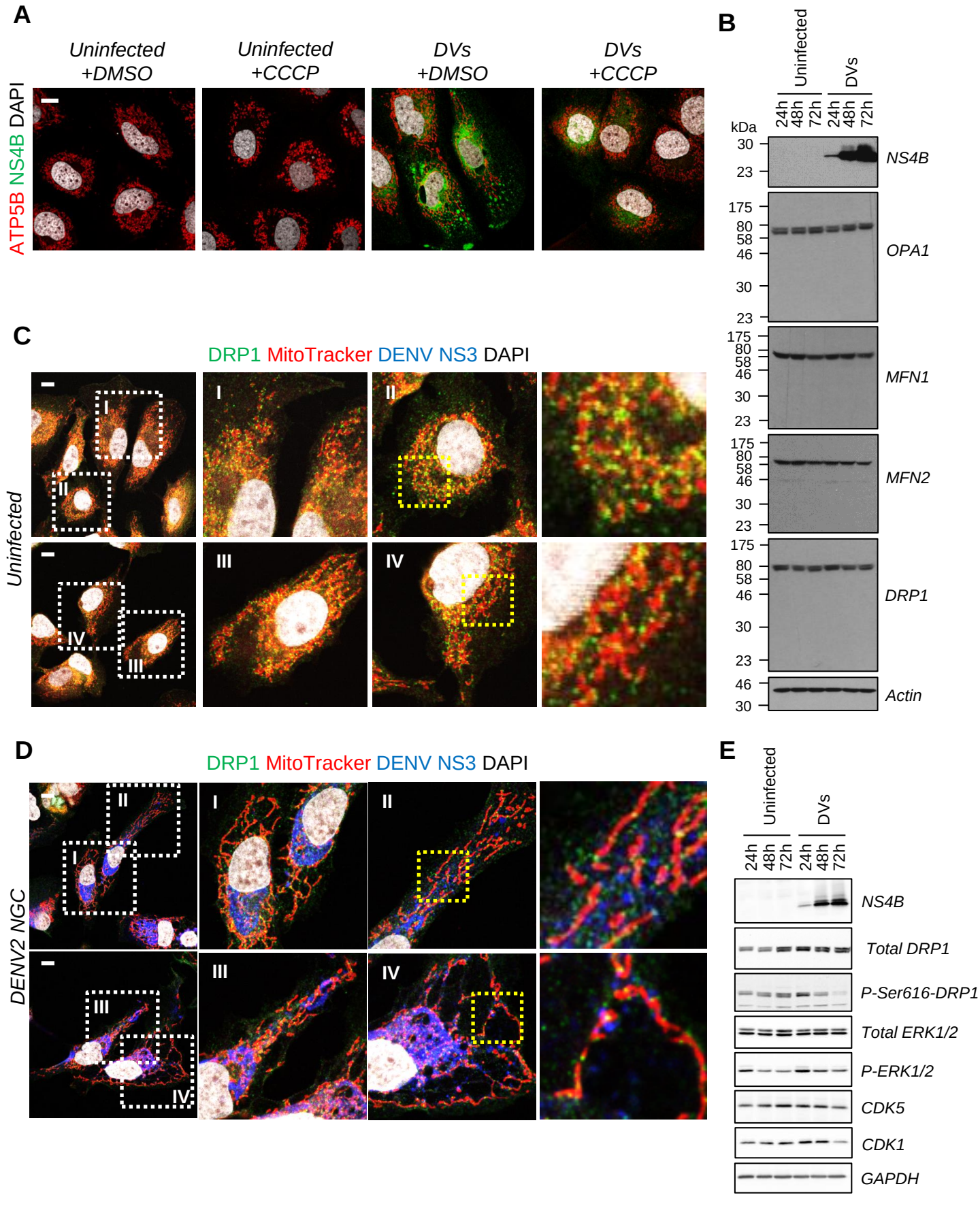
A
Uninfected +DMSO
Uninfected +CCCP
DVs +DMSO
DVs +CCCP
ATP5B NS4B DAPI
B
Uninfected
DVs
24h 48h 72h 24h 48h 72h
kDa
NS4B
OPA1
MFN1
MFN2
DRP1
Actin
C
DRP1 MitoTracker DENV NS3 DAPI
Uninfected
D
DRP1 MitoTracker DENV NS3 DAPI
DENV2 NGC
E
Uninfected
DVs
24h 48h 72h 24h 48h 72h
NS4B
Total DRP1
P-Ser616-DRP1
Total ERK1/2
P-ERK1/2
CDK5
CDK1
GAPDH

Figure S7

SUPPLEMENTAL INFORMATION

SUPPLEMENTAL FIGURE LEGENDS

Figure S1: Purification and identification of NS4B-associated host factors (related to Figure 1). (A) Schematic representation of the DENV2 16681s genomes expressing wt (DVs) or HA-tagged NS4B (DVs(NS4B-HA*)). Black lines represent 5' and 3' non translated regions (NTR). (B) Huh7 cells were infected with DVs or DVs(NS4B-HA*) virus stocks (MOI=5). Forty-eight hours later, cell extracts were prepared and subjected to immunoprecipitation using HA-specific antibodies. Cell extracts and immune complexes were analyzed by Western blotting with NS4B-specific antibodies. (C) Immunoprecipitates shown in (B) were analyzed using silver staining. • indicates proteins specifically co-purified with NS4B-HA* (indicated with the arrow). (D) Host proteins contained in NS4B-specific immunocomplexes were identified by GeLC-MS/MS using triplicate samples prepared as shown in (B) and (C). NS4B interactants were considered specific when enriched more than 8-fold ($p \leq 5x10^{-2}$) relative to the technical background that was determined with the DENV genome encoding the parental (non-tagged) NS4B (DVs). Mitochondrial proteins are written in red. Values were derived from three independent experiments. A complete list of the hits is given in Table S1. (E) Huh7 cells were infected with DVs or DVs(NS4B-HA*) virus stocks (MOI=1). Seventy-two hours later, cell extracts were prepared and subjected to HA-specific immunoprecipitation. Cell extracts and immune complexes were analyzed using Western blotting and the mitochondrial proteins ATP5B, MAOB and VDAC2 were validated as NS4B-interacting proteins. (F) Huh7 cells were infected with the DENV2 strain 16681 (DVs; MOI=1) or left uninfected. Three days later, cells were fixed, permeabilized and MAOB and NS4B were visualized by immunofluorescence using confocal microscopy. Scale bar: 10 µm.

Table S1: Mass spectrometry analysis of NS4B-HA*-containing protein complexes purified from DENV-infected cells (related to Figure 1). Host proteins contained in HA-specific immunocomplexes prepared from DVs- and DVs(NS4B-HA*)-infected cells were identified by GeLC–MS-MS using triplicate samples (EXP 1, EXP 2, EXP 3). For each identified protein, the ENSEMBL ID and the number of detected peptides in each replicate are shown. Enrichment factor (Log2 Fold Change) and significance for each identified protein were determined. NS4B-HA* interactants were considered specific when enriched more than 8-fold ($p \leq 5x10^{-2}$) relative to the technical background (DVs).

Movie S1: This movie shows fixed DENV2 DVs-infected Huh7 cells which were stained three days post-infection for mitochondria (red), NS3 (blue) and NS4B (green) and analyzed by confocal microscopy (related to Figure 1). Optical sections were acquired with a spinning disc confocal microscope and after deconvolution, Z-stacks were used for 3D reconstruction. The movie was generated with the Imaris 8 software package and shows the proximity of NS3/NS4B-containing punctae to DENV-induced elongated mitochondria.

Figure S2: All four DENV serotypes and ZIKV induce mitochondria elongation, but not WNV and HCV (related to Figure 1). Huh7 cells were infected at MOI=1-5 with (A) DVs, (B) DENV1 Hawaii, (C) DENV2 New Guinea C (NGC) strain, (D) DENV3 H87, (E) DENV4 H241, (F) ZIKV H/PF/2013, (G) ZIKV MR766, (H) WNV NY99 or (I) HCV Jc1. Thirty-six hours (NGC), 48 hours (WNV, ZIKV MR766, HCV) or 72 hours post-infection (all other samples), cells were incubated with MitoTracker, fixed, permeabilized and indicated proteins and dsRNA were visualized by immunofluorescence using confocal microscopy. Scale bar: 10 µm. (J) Quantification of the impact of virus infection on mitochondria morphology. The mitochondrial network of ~100 cells per condition and experiment (n=2-6) was examined and classified into three morphological categories (normal, fragmented, elongated) as described in supplemental experimental procedures.

Movie S2: Live cell imaging of Huh7-mito-mTurquoise2 cells left uninfected (left panel) or infected with DENV2 DVs (MOI=10; right panel) (related to Figure 1). Every hour, the signal in the Cyan channel was acquired. Time and scale bar are indicated in the movie. The movie shows time-dependent DENV-induced elongation of mitochondria until cell death because of cytopathic effects caused by DENV.

Movie S3: Live cell imaging of Huh7-mito-mTurquoise2 cells infected with DENV2 NGC (MOI=10) (related to Figure 1). The signal in the cyan channel was acquired every hour. Time post-infection and scale bar are indicated in the movie. The movie shows time-dependent DENV-induced elongation of mitochondria until cell death because of cytopathic effects caused by DENV.

Figure S3: Establishment of a stable Huh7 cell line suitable for visualization of mitochondria and ER in live cells (related to Figures 1 and 2). (A) Huh7 cells stably expressing the mTurquoise2 fluorophore fused with the

COX8 mitochondria-targeting signal (mito-mTurquoise2) were generated by lentiviral transduction. Cells were infected with the reporter virus DVs-R2A (MOI=0.1) and Renilla luciferase activity (RLU), used as a readout of DENV replication, was measured 24, 48 and 72 hours post-infection (hpi). Note that the reporter cells support DENV replication comparably to the parental non-transduced cells. AU: arbitrary units. (B) Huh7-mito-mTurquoise2 cells were infected with DVs (MOI=1). Three days post-infection, cells were fixed, permeabilized and NS3 was detected by immunofluorescence using confocal microscopy. Scale bar: 10 µm. (C) Live cell imaging frame captures of uninfected Huh7-mito-mTurquoise2 cells. Captures were made 20, 28, 36, 44 and 52 hours after a two-hour mock-infection and show a normal mitochondrial network. To facilitate tracking, two cells of interest are labeled with α and β. Scale bar: 10 µm. (D) Huh7 cells stably expressing mito-mTurquoise2 and YFP-Sec61β were generated by lentiviral transduction. Cells were infected with the DENV reporter virus DVs-R2A (MOI=0.1). Renilla luciferase activity (RLU) was measured 24, 48, 72 and 96 hours post-infection. Note that the simultaneous expression of the two fluorophore reporters has little effect on permissiveness to DENV. (E) Cells were infected with DVs (MOI=1). Three days later, cells were, fixed, permeabilized and NS3 was detected by immunofluorescence using confocal microscopy. Note the punctate staining pattern of NS3 that overlaps perfectly with YFP-Sec61β. Scale bar: 10 µm.

Movie S4: Three-dimensional reconstruction of the mitochondrial network in a DENV2 NGC-infected Huh7 cell (24 hours post infection; MOI=5) using focused ion beam/scanning electron microscopy (FIB/SEM) (related to Figure 2). Images of transversal sections of approximately 10 nm were acquired and used for 3D reconstruction. Reconstructed mitochondria are shown in red and DENV convoluted membranes in green. Note the elongated mitochondrial network with CMs in close proximity to mitochondria. Scale bar: 5 µm.

Figure S4: DENV-induced mitochondria elongation occurs in the vicinity of convoluted membranes (related to Figure 2). (A) Huh7 cells were infected with DVs (MOI=1) or left uninfected. Three days later, cells were processed for FIB/SEM as described in the Methods Online section. 3D reconstruction for mitochondria (red) and CM (green) was performed. Scale bar: 2 µm. (B) Sections of DVs-infected cells were analyzed with TEM. Magnification of regions of interest (red squares) are shown in the respective right panels to highlight that ER-mitochondria contact sites are partially disrupted in DENV-infected cells and that ER membranes are connected to CMs (red arrows). Yellow arrows indicate DENV-induced vesicle packets (VP). M: mitochondria.

Figure S5: DENV infection alters mitochondria-ER contacts (related to Figure 2). Huh7/mito-mTurquoise2/YFP-Sec61β cells were left uninfected (A) or infected with DVs (B). Three days later, cells were fixed and stained for NS3 (not shown). Optical sections were acquired with a spinning disc confocal microscope and after deconvolution, Z-stacks were used for 3D reconstruction and 3D colocalization analysis between mitochondria and YFP-Sec61β-signals (note that NS3-positive cells were considered infected). I-II: Magnifications of regions of interest show the mitochondria-ER contacts. White areas on reconstructed mitochondria (Coloc.) indicate regions of colocalization with YFP-Sec61β. White scale bar: 1 µm. (C-E) CLEM of a DVs-infected cell using YFP-Sec61β as a marker of NS3/NS4B-containing puncta. Mito-mTurquoise2/YFP-Sec61β-expressing cells were infected with DVs and processed for CLEM three days post-infection. The selected fixed cell was subjected to optical sectioning using a confocal microscope. (C) The 20x low magnification image of a combined phase contrast/fluorescence picture displays the cell of interest (white square) selected for high resolution analysis and shows the coordinate (Letter N) in the background. The mitochondria marker and YFP-Sec61β puncta are shown in red and green, respectively. (D) Combination of phase contrast and fluorescence images of the selected cell. (E) Superposition of a low magnification TEM image with the confocal microscopy Z-stack. Mitochondria were used to allocate the red fluorescent signal of a Z-stack to the proper ultrastructure and hence, for overall correlation. Higher resolution images of this cell are shown in Figure 3D-F.

Movie S5: Live cell imaging of uninfected Huh7/mito-mTurquoise2/YFP-Sec61β cells (related to Figure 3). Every hour, the signals in the Cyan and YFP channels were acquired. The movie shows the dynamics of the mitochondrial network. No accumulation of YFP-Sec61β punctae could be observed. Time and scale bar are indicated in the movie. Left: Combined imaging of both YFP-Sec61β and mito-Turquoise2. Right: Imaging of YFP-Sec61β only.

Movie S6: Live cell imaging of Huh7/mito-mTurquoise2/YFP-Sec61β cells infected with DVs (MOI=10) (related to Figure 3). Every hour, the signals in the Cyan and YFP channels were acquired. The movies show the dynamics of the mitochondrial network. The bottom movie highlights the continuous contacts between elongated mitochondria and CMs during infection. It also pinpoints the dynamic features of CMs undergoing merging and

division events (still images shown in Figure S6A). Time post-infection and scale bar are indicated in the movies. Left: Combined imaging of both YFP-Sec61β and mito-Turquoise2. Right: Imaging of YFP-Sec61β only. Still images of the top movie are shown in Figure S6B.

Figure S6: DENV-induced CMs are highly dynamic but remain in close proximity of mitochondria and ZIKV replication is influenced by DRP1 expression (related to Figures 3 and 5). Huh7/mito-mTurquoise2/YFP-Sec61β cells were infected with DVs (MOI=10) and analyzed by live-cell imaging. (A) Series of still images (from Movie S6, bottom) pinpointing the dynamic features of CMs. Within the same infected cell, division (red arrows) and merging (blue arrows) of CMs can be observed. Time points after infection are indicated in the top; images were taken every hour. (B) Time series of a cell of interest highlighting that CMs and mitochondria remain in close proximity throughout the observation period (from Movie S6, top). Scale bar: 10 µm. (C) Huh7 and Huh7.5 cells were transduced with shRNA-expressing lentiviruses and infected two days later with ZIKV MR677 (MOI=0.05) or HCV JcR2A (MOI=0.1), respectively. Two days post-infection, ZIKV titers and Renilla luciferase activity (RLU) reflecting HCV RNA replication were determined. Mean values of three (ZIKV) or two (HCV) independent experiments and corresponding SEM are shown. Related to Figure 5.

Figure S7: DENV infection does not affect the expression levels of the mitochondria fusion or fission factors while impeding DRP1 translocation to mitochondria (related to Figure 6). (A) Mitochondria elongation is important for the maintenance of DENV-induced CMs. Huh7 cells were infected with DVs at a MOI of 1 or left uninfected. Two days post-infection, cells were treated with 30 µM CCCP for 4 hours at 37^{o}C. After fixation and permeabilization, ATP5B and NS4B were detected by immunofluorescence using confocal microscopy. Scale bar: 10 µm. (B) Huh7 cells were infected with DVs (MOI=1) or left uninfected. At given time points after infection, cell extracts were prepared and analyzed by Western blotting using NS4B-, OPA1-, MFN1-, MFN2- and DRP1-specific antibodies. Actin detection was used to control for comparable protein amounts loaded onto each lane of the gel. (C-D) Huh7 cells were left uninfected (C) or infected with DENV2 NGC (MOI=5) (D). Thirty-six hours post-infection, cells were labeled with MitoTracker as well as DRP1- and NS4B-specific antibodies. Nuclear DNA was stained with DAPI. The white squares designate magnified regions of interest shown in the right of each panel. Further magnification of these images is indicated with yellow squares and shown on the right of each respective panel. Scale bar: 10 µm. (E) Huh7 cell extracts were generated exactly as in (B) and analyzed for the indicated proteins by Western blotting.

SUPPLEMENTAL EXPERIMENTAL PROCEDURES

Cell lines and virus strains

Huh7, 293T, VeroE6, HeLa and A549 cells were all cultured in Dulbecco's modified Eagle medium (DMEM, Life Technologies) containing 10% fetal bovine serum, 100 U/mL penicillin, 100 µg/mL streptomycin and 1% non-essential amino acids (complete DMEM). Stable Huh7 cell lines were cultured in medium containing either 2 ug/mL zeocin or 1ug/mL puromycin or both. DENV2 DVs virus stocks were prepared exactly as described earlier (Chatel-Chaix et al., 2015; Fischl and Bartenschlager, 2013) by electroporation of BHK-21 cells with in vitro transcribed DENV2 RNA and subsequent virus amplification in VeroE6 cells. DENV1 Hawaii, DENV2 New Guinea C (NGC), DENV3 H87, DENV4 H241, ZIKV H/PF/2013, ZIKV MR766 WNV NY99 virus stock were prepared by virus amplification in VeroE6 cells or insect C6/36 cells. All virus stocks were titrated using plaque assays.

Reagents

Carbonyl cyanide 3-chlorophenylhydrazone (CCCP) was obtained from Sigma-Aldrich. Production and characterization of rabbit anti-DENV NS3, anti-DENV NS4B, anti-DENV NS4A and anti-HCV NS3 were previously reported (Miller et al., 2006; Miller et al., 2007; Welsch et al., 2009; Koch and Bartenschlager, 1999). Mouse anti-DENV NS3 was obtained from GeneTex. All AlexaFluor-conjugated secondary antibodies and MitoTracker Red CMXRos were purchased from Life Technologies. Mouse anti-DRP1 and anti-OPA1 antibodies were purchased from BD Biosciences, mouse anti-MFN2, mouse anti-GAPDH and goat anti-MAOB antibodies from Santa Cruz Biotechnology, mouse anti-MFN1, rabbit anti-VDAC2, mouse anti-ATP5B and mouse anti-DENV NS1 antibodies from Abcam, mouse anti-β-actin and mouse anti-HA antibodies from Sigma-Aldrich, rabbit anti-phospho-Ser616-DRP1, rabbit anti-ERK1/2, rabbit anti-phospho-Thr201/Tyr204 ERK1/2, anti-phospho-Ser637-DRP1 and anti-COX IV antibodies from Cell Signaling, rabbit anti-calnexin from Stressgen, rabbit anti-FACL4

from BioCat, mouse anti-RIG-I from Alexis and mouse J2 anti-dsRNA antibodies from Scicons (English and Scientific Consulting Kft.).

DNA cloning

The plasmids containing the DENV2 16681s-based sequences of the full-length wild-type virus (pFK-DVs), the NS4B-HA-encoding virus, the Renilla luciferase (Rluc) reporter virus (pFK-DVs-R2A) and the sub-genomic reporter replicon (pFK-sgDVs-R2A) were described elsewhere (Chatel-Chaix et al., 2015; Fischl and Bartenschlager, 2013). The construction of pWPI-NS2B-3 and pTM-based expression plasmids encoding DENV HA-tagged NS4A, 2K-NS4B, NS4A-2K-NS4B and HCV JFH-1 NS3-5B polyprotein was previously reported (Chatel-Chaix et al., 2015; Reiss et al., 2011). Note that the 2K sequence in 2K-NS4B serves as signal peptide for NS4B membrane insertion; 2K is removed by the signalase generating mature NS4B. The construction of pWPI-mito-mTurquoise2 will be described elsewhere (A.R. and K. Rohr, in preparation). For lentiviral constructs expressing DENV2 proteins, sequences corresponding to NS4A, NS4B, 2K-NS4B and NS4A-2K-NS4B were amplified using PCR and pTM-based expression plasmids (Chatel-Chaix et al., 2015) as templates. PCR products were inserted into the BamHI/SpeI cassette of the pWPI plasmid. pENTR221-hDNM1L (a kind gift of Dr. Nathan R. Brady) was used to shuttle the human DRP1 coding sequence into pWPI-HA-puro using the Gateway recombination system (Life Technologies).

Co-immunoprecipitation assays and mass spectrometry

Co-immunoprecipitations were performed exactly as described previously (Chatel-Chaix et al., 2013). In brief, infected cells were lysed with dodecyl-β-maltoside-containing buffer and subjected to immunoprecipitation using anti-HA agarose beads (Sigma-Aldrich). For Western blot analysis, purified material was eluted with PBS containing 5% SDS and concentrated by acetone-mediated precipitation. For mass spectrometry-based identification of NS4B interactors, purified proteins were collected by three successive elutions using 100 µL of a 100 ng/µL HA peptide solution (Sigma-Aldrich). Pooled eluates were concentrated by acetone-mediated precipitation and submitted to GeLC-MS/MS (performed by the proteomics platform of the Institute of Microbiology, University of Greifswald, Germany). Protein composition of the resulting samples was determined using X!Tandem (version 2013.06.15). P-values from spectral counts were computed using the R/Bioconductor package DESeq and adjusted for multiple testing by the method of Benjamini-Hochberg (Benjamini and Hochberg, 1995). A cellular protein was considered as a NS4B interaction partner when it was significantly enriched more than 8-fold ($p \leq 5x10\text{-}2$) relative to the negative control which corresponded to cells infected with the non-tagged NS4B DENV that were processed in parallel.

Indirect immunofluorescence and confocal microscopy

Cells grown on coverslips were washed twice, fixed with PBS containing 4% paraformaldehyde for 20 minutes and permeabilized with 0.2% Triton-X100 in PBS. Coverslips were subjected to blocking with PBS containing 5% bovine serum albumin (BSA) and 10% goat serum. After washings, the cells were incubated with primary antibodies diluted in PBS/5% BSA for two hours. After three washes with PBS, cells were subjected to one-hour incubation with AlexaFluor 488-, 568-, or 647-conjugated secondary antibodies. Cells were washed three times with PBS for 15 minutes each and nuclei were stained with DAPI for 10 minutes. Coverslips were mounted on slides with FluoromountG (Southern Biotechnology Associates) and examined with a Leica SP2 laser scanning confocal microscope (Leica). For the quantification of mitochondria phenotypes, cells were observed with an inverted light microscope. The mitochondrial network of at least 100 cells per condition and experiment (2-6 independent replicates per virus) was examined and classified into three distinct categories (normal, fragmented and elongated morphology). A mitochondrial network was considered elongated when the elongation was observed at the whole cell level with at least 5 mitochondria longer than 15 µm (corresponding to the approximate diameter of a Huh7 cell nucleus). Mitochondria were classified as fragmented when $\geq$ 75 % of mitochondria appeared homogenously circular and with a diameter of ~1 µm in a dot-like pattern with no sign of elongation. Optical sections of 130 nm thickness were acquired with a Nikon TE2000-E inverted confocal microscope equipped with an Ultraview ERS spinning disc (PerkinElmer Life Sciences). Acquired pictures were subjected to deconvolution using Autoquant X3 software (Media Cybernetics). Three-dimensional reconstruction of cells and subsequent colocalization analyses were performed using the deconvolved Z-stacks and the Imaris 8 software package (Bitplane). For the analysis of NS4B-positive puncta (Figure 5J-K), cells were transduced with shRNA-expressing lentivirus and transfected three days later with plasmids encoding the DENV2 NS1-5 polyprotein. Fixed cells were labeled for immunofluorescence as described above. Optical sections of 300 nm thickness were acquired with a Leica SP8 inverted confocal

microscope using a 63x Plan-Apo N.A. 1.4 objective. Image analysis was performed using the Imaris 8 software package (Bitplane). Surface items were calculated on the NS4B signal using an absolute intensity thresholding of 30.8032. All surfaces smaller than 0.1 μm^2 were excluded. The average volume and the total number of surfaces for each cell were recorded.

Immuno-gold labelling

To fix the cells, one volume of 0.2 M PHEM buffer (120 mM PIPES, 50 mM HEPES, 4 mM $MgCl_2$, 20 mM EGTA, pH 6.9) containing 8% paraformaldehyde and 0.2% glutaraldehyde was added to the culture medium. Cells were incubated for 10 minutes at room temperature. After a second fixation for one hour with 0.1 M PHEM containing 4% paraformaldehyde and 0.1% glutaraldehyde, cell were stored in 0.1 M PHEM/4% paraformaldehyde at 4°C. Cells were washed for 10 minutes in 0.1 M PHEM/50 mM glycine and collected in 0.1 PHEM containing 1% gelatin. Cells were centrifuged, resuspended in pre-warmed 10% gelatin and spun down again. Cells were incubated on ice until the gelatin had solidified. Excess of cell-free gelatin was trimmed away and gelatin-embedded cells were cut into small cubes under a magnifying glass. The cubes were put into a 2.3 M sucrose solution and spun at 4°C overnight. Cell pellets were mounted on silver pins, flash-frozen and stored in liquid nitrogen. Samples were sectioned with a Reichert Ultracut S ultramicrotome using a Reichert FCS cryo-attachment and a Diatome diamond knife (Diatome). Cryosections were thawed and immunolabelled as previously described (Griffiths et al., 1983; Paul et al., 2013) using mouse anti-HA (Sigma-Aldrich) or immune-purified rabbit anti-NS3 primary antibodies (Welsch et al., 2009). Samples were examined using an EM-10 transmission electron microscope (Zeiss) with a built-in MegaView camera (Olympus).

Focused ion beam - scanning electron microscopy

Huh7 cells were infected with DENV (strains NGC and DVs; MOI 5) and fixed with 2.5% glutaraldehyde (Electron Microscopy Sciences) and 0.1% malachite green oxalate (Sigma) in 0.1 M PHEM buffer. Cells were washed with 0.1 M PHEM buffer and stored at 4°C until further processing in a PELCO BioWave Pro microwave processor (Ted Pella, Inc.). For post-fixation samples were incubated with 1% osmium tetroxide (Electron Microscopy Sciences) and 0.8% potassium hexacyanoferrate(III) ($K_3Fe(CN)_6$; Merck) in 0.1 M PHEM. Cells were rinsed with 0.1 M PHEM, incubated with 0.5% uranyl acetate in water, rinsed with water, dehydrated with increasing concentrations of ethanol (25, 50, 75, 90 and 100%) and embedded with a graded series of Epon (Serva). Epon-infiltrated cells were incubated at 55°C to polymerize the resin. The part of the resin block containing the cells was mounted onto a SEM stub (Agar Scientific) using carbon sticker (Plano, GmBH, Wetzlar) and surrounded with silver paint (Pelco Colloidal Silver, Ted Pella Inc.) with the cells pointing upwards, perpendicular to the electron column. Samples were sputter-coated with gold (Quorum, GaLa Instrumente GmbH) for 120 sec at 30 mA. Images were recorded with a dual beam Auriga 60 FIB-SEM microscope (ZEISS), equipped with a gallium ion source for focused ion beam milling and a field emission gun scanning electron microscope. The specimen stage was tilted to 54° and exposed to the focused ion beam in a way that the stage of the plane was parallel to the ion beam. Prior to milling and imaging, the sample surface was coated with platinum (~1 µm) using the gas injection system to cover the region of interest (on average 50 μm^2). All sample preparation and acquisition settings were performed using the Atlas3D software package (FIBICS Inc.). A cross sectional cut was introduced in two stages. First, a cut was made at high beam current (typically 16 nA) and at an accelerating voltage of 30 kV to create a trench that enabled viewing of the cross-section. In the second step, the ion beam was scanned using a current of 2 nA to polish and smooth the surface. SEM imaging was done using the ESB (back-scattered electron) detector at 1.5 kV, with a pixel size of 10 nm in x/y. For slice-and-view image series, a z-step of ~10 nm was chosen to remove the material from the specimen surface with the focused ion beam in order to obtain isotropic datasets. All acquired images were combined as a stack using the FIJI (ImageJ) software package and aligned using the TrakEM2 plugin. Finally, the contrast of all images was inverted to obtain the contrast of conventional TEM images. Organelles of interest were rendered using the IMOD software package (version 4.7).

Transfection

Electroporation of Huh7 cells with in vitro transcripts of DENV genomes was performed exactly as described earlier (Chatel-Chaix et al., 2015). Huh7 cells stably expressing T7 RNA polymerase and in some experiments in addition the NS2B-NS3 protease (Chatel-Chaix et al., 2015) were grown on glass coverslips and transfected with pTM-based plasmids using TransIT-LT1 (Mirus) according to the manufacturer's instructions. Culture medium was changed 4 hours later. Cells were processed for indirect immunofluorescence 24 hours post-transfection.

Lentivirus production and transduction of cells

Stable knock-down of selected genes and overexpression of DENV proteins was achieved through transduction with lentiviruses encoding distinct shRNAs and proteins, respectively. For production of lentivirus stocks, sub-confluent 293T cells were transfected with packaging plasmids pCMV-Gag-Pol and pMD2-VSV-G (kind gifts from Dr. Didier Trono) and shRNA-encoding pLKO-puro plasmids obtained from Sigma-Aldrich or pWPI-based plasmids using 25 kD linear polyethylenimine (Polysciences Inc.) as previously described (Chatel-Chaix et al., 2013). Two days post-transfection, lentivirus-containing medium was collected and filtered. Lentiviruses were titrated by transducing HeLa cells and subsequent treatment with 1 ug/ml puromycin. Five days later, cells were fixed and stained with 1% crystal violet/10% ethanol for 15-30 minutes. Stained cells were rinsed with water, colonies were counted and titers calculated taking into account inoculum dilution. For all experiments, transductions were typically performed using a MOI of 5 for Huh7 or 3 for A549 cells in the presence of 4 µg/mL polybrene. The pLKO plasmids TRCN0000001097 and TRCN0000082686 (Sigma Aldrich) were used to knockdown the expression of DRP1 and MFN2, respectively. The non-targeting shRNA-encoding plasmid SHC002 (Sigma-Aldrich) was used as negative control and reference. Cell viability of transduced cells was evaluated using the CellTiter-Glo Luminescent Cell Viability Assay kit (Promega) measuring ATP amounts according to the manufacturer's instructions. Luminescence was measured with a Mithras LB940 plate reader (Berthold Technologies). The same transduction approach was used to produce Huh7 cells expressing YFP-tagged Sec61β and mitochondria-targeted mTurquoise2. Cells expressing the latter were selected with 2 µg/ml zeocin and then, transduced with YFP-Sec61β-encoding lentiviruses. After double selection with 1 µg/mL puromycin and 2 µg/mL zeocin, cells were used for CLEM. For live cell imaging analyses, cells expressing high levels of these markers were sorted using flow cytometry prior to expansion.

Virus titration and replication measurement

Titers of infectious virus were determined using plaque assays as previously described (Metz et al., 2015). In brief, VeroE6 cells were infected with virus preparations that had been serially diluted in complete DMEM. Approximately two hours post-infection, the inoculum was removed and cells were cultured at 37˚C with serum-free MEM (Life Technologies) containing 1.5% carboxymethylcellulose. Several days post-infection (depending on the virus strain), cells were fixed by 2 hours incubation with formaldehyde (5% final concentration). After extensive washes with water, cells were stained with 1% crystal violet/10% ethanol for 15-30 minutes. Stained cells were rinsed with water, plaques were counted and titers of infectious virus were calculated. RNA replication of DENV2 (DVs-R2A) reporter virus was determined by measuring the activity of virus-encoded Renilla luciferase (Rluc) exactly as previously described (Chatel-Chaix et al., 2015; Fischl and Bartenschlager, 2013). After lysis of the cells, coelenterazine (1.43 µM final concentration) was added and luminescence was measured using a Lumat LB9507 luminometer (Berthold Technologies).

Real-time RT-PCR

Total RNA was purified from cells using the Nucleospin RNA isolation kit (Macherey-Nagel) according to the instructions of the manufacturer. cDNAs were generated using the High Capacity cDNA Reverse Transcription kit (Applied Biosystems) and used for real-time PCR with the iTaq Universal SYBR Green kit (Bio-Rad) and the following specific primer pairs: GAAGGTGAAGGTCGGAGTC and GAAGATGGTGATGGGATTTC for GAPDH; AGCACTGTGTTGGCGTACAG and GACTTCGAGCAAGAGATGG for β-actin; GAAGCAGGCAATCACAGAAA and TGAAACCGACCATAGTGGAA for ISG56; CAGCTCCAAGAAAGGACGAAC and GGCAGTGTAACTCTTCTGCAT for IFN-β; GCAGGTTCAAATCTCTGTCACC and AAGACAGGAGAGCTGCAACTC for IFN-λ1 (Bender et al., 2015). Amplification reactions and measurements were carried out using a C1000 Touch Thermal cycler (CFX96 realtime system; Bio-Rad).

Generation of RIG-I knockout cell lines using CRISPR/Cas9 technology

Knock-out of RIG-I in Huh7 cells was achieved by using the CRISPR/Cas9 system as previously described (Shalem et al., 2014). In brief, two different single-guide RNAs (sgRNAs) were designed targeting the second exon of the coding region of RIG-I with the help of the open source tool (Heigwer et al., 2014) and inserted into the lentiviral vector lentiCRISPR v2 (Addgene #52961) also encoding the Cas9 nuclease. The following sgRNAs were used: 5'

CTGTTGGAGCTCCAGGAGGA 3' (KO-1) and 5' TGGAGCTCCAGGAGGAAGGC 3' (KO-2). Lentiviruses were produced as described above and used to transduce Huh7 cells. Cell populations were selected with 1 ug/mL puromycin and tested for RIG-I expression using Western blotting.

Sub-cellular fractionation and MAM isolation

The procedure used to isolate mitochondria-associated membranes (MAMs) was previously described (Horner et al., 2011; Neufeldt et al., 2013; Neufeldt et al., 2016; Wieckowski et al., 2009). Briefly, cells were lysed using a Balch homogenizer (Isobiotec) followed be removal of nuclei and cellular debris by low speed centrifugation. Mitochondria and associated membranes were then pelleted from the supernatant and MAMs were separated from the mitochondria by centrifugation through a percoll gradient. Total protein amount in each fraction was determined using Bradford assays. Protein contents were evaluated by SDS-PAGE and Western blotting. FACL4 and calnexin were used as marker enriched in the MAM fraction and α-tubulin as a cytosolic marker.

Statistical analysis

Standard deviation (SD) (on representative experiments) was calculated using at least three technical replicates. Standard error to the mean (SEM) was determined based on at least three independent experimental replicates (except if stated otherwise). Statistical significance was evaluated by determining p-values using the Student's t-Test (two-tailed distribution). A result was considered significant when the p-value was below 0.05.

SUPPLEMENTAL REFERENCES

Bender,S., Reuter,A., Eberle,F., Einhorn,E., Binder,M., and Bartenschlager,R. (2015). Activation of Type I and III Interferon Response by Mitochondrial and Peroxisomal MAVS and Inhibition by Hepatitis C Virus. PLoS. Pathog. *11*, e1005264.

Benjamini,Y. and Hochberg,Y. (1995). Controlling the false discovery rate: a practical and powerful approach to multiple testing. Journal of the Royal Statistical Society. Series B *57*, 289-300.

Chatel-Chaix,L., Germain,M.A., Motorina,A., Bonneil,E., Thibault,P., Baril,M., and Lamarre,D. (2013). A host YB-1 ribonucleoprotein complex is hijacked by hepatitis C virus for the control of NS3-dependent particle production. J. Virol. *87*, 11704-11720.

Fischl,W. and Bartenschlager,R. (2013). High-throughput screening using dengue virus reporter genomes. Methods Mol. Biol. *1030*, 205-219.

Griffiths,G., Simons,K., Warren,G., and Tokuyasu,K.T. (1983). Immunoelectron microscopy using thin, frozen sections: application to studies of the intracellular transport of Semliki Forest virus spike glycoproteins. Methods Enzymol. *96*, 466-485.

Heigwer,F., Kerr,G., and Boutros,M. (2014). E-CRISP: fast CRISPR target site identification. Nat. Methods *11*, 122-123.

Koch,J.O. and Bartenschlager,R. (1999). Modulation of hepatitis C virus NS5A hyperphosphorylation by nonstructural proteins NS3, NS4A, and NS4B. J. Virol. *73*, 7138-7146.

Metz,P., Chiramel,A., Chatel-Chaix,L., Alvisi,G., Bankhead,P., Mora-Rodriguez,R., Long,G., Hamacher-Brady,A., Brady,N.R., and Bartenschlager,R. (2015). Dengue Virus Inhibition of Autophagic Flux and Dependency of Viral Replication on Proteasomal Degradation of the Autophagy Receptor p62. J. Virol. *89*, 8026-8041.

Miller,S., Sparacio,S., and Bartenschlager,R. (2006). Subcellular localization and membrane topology of the Dengue virus type 2 Non-structural protein 4B. J. Biol. Chem. *281*, 8854-8863.

Neufeldt,C.J., Joyce,M.A., Levin,A., Steenbergen,R.H., Pang,D., Shields,J., Tyrrell,D.L., and Wozniak,R.W. (2013). Hepatitis C virus-induced cytoplasmic organelles use the nuclear transport machinery to establish an environment conducive to virus replication. PLoS. Pathog. *9*, e1003744.

Neufeldt,C.J., Joyce,M.A., Van,B.N., Levin,A., Kirkegaard,K., Gale,M., Jr., Tyrrell,D.L., and Wozniak,R.W. (2016). The Hepatitis C Virus-Induced Membranous Web and Associated Nuclear Transport Machinery Limit Access of Pattern Recognition Receptors to Viral Replication Sites. PLoS. Pathog. *12*, e1005428.

Paul,D., Hoppe,S., Saher,G., Krijnse-Locker,J., and Bartenschlager,R. (2013). Morphological and biochemical characterization of the membranous hepatitis C virus replication compartment. J. Virol. *87*, 10612-10627.

Reiss,S., Rebhan,I., Backes,P., Romero-Brey,I., Erfle,H., Matula,P., Kaderali,L., Poenisch,M., Blankenburg,H., Hiet,M.S., Longerich,T., Diehl,S., Ramirez,F., Balla,T., Rohr,K., Kaul,A., Buhler,S., Pepperkok,R., Lengauer,T., Albrecht,M., Eils,R., Schirmacher,P., Lohmann,V., and Bartenschlager,R. (2011). Recruitment and activation of a lipid kinase by hepatitis C virus NS5A is essential for integrity of the membranous replication compartment. Cell Host. Microbe *9*, 32-45.

Shalem,O., Sanjana,N.E., Hartenian,E., Shi,X., Scott,D.A., Mikkelsen,T.S., Heckl,D., Ebert,B.L., Root,D.E., Doench,J.G., and Zhang,F. (2014). Genome-scale CRISPR-Cas9 knockout screening in human cells. Science *343*, 84-87.

Wieckowski,M.R., Giorgi,C., Lebiedzinska,M., Duszynski,J., and Pinton,P. (2009). Isolation of mitochondria-associated membranes and mitochondria from animal tissues and cells. Nat. Protoc. *4*, 1582-1590.